

# The Effect of Rock Mass Confinement on the Bond Strength of Fully Grouted Cable Bolts

A. J. HYETT†  
W. F. BAWDEN†  
R. D. REICHERT†

*A laboratory and field research programme was conducted to investigate the major factors influencing the bond capacity of grouted cable bolts. All tests were conducted on standard 5/8" (15.9 mm) 7-strand cable grouted using type 10 Portland cement pastes. The results indicate that cable bolt capacity most critically depends on:*

- (i) *the cement properties, which are primarily controlled by water : cement ratio;*
- (ii) *the embedment length; and*
- (iii) *the radial confinement acting on the outer surface of the cement annulus.*

*The material properties of cement paste vary with the water : cement ratio of the mix. The use of low water : cement ratio grouts (< 0.40 by wt) can increase peak cable bolt capacities by 50–75%. This can be attributed to both their high uniaxial compressive strengths and their high Young's moduli. The effect is maximized under conditions of high radial confinement. However, the use of super-thick pastes (0.30 and less) may be both impractical and undesirable, first because of their limited pumpability and second because of their inconsistency in strength.*

*Tests at different embedment lengths indicated that cable bolt capacity increased with embedment length although not in direct proportionality. All tests were conducted with embedment length: cable diameter ratios in excess of 15 (below 5 the decay in shear stress along the cable can be ignored). Consequently, failure is non-simultaneous in nature, with one section having failed while another is approaching peak capacity.*

*In the laboratory "split-pipe" tests were conducted using PVC, Al and steel pipes to provide radial confinement, and in the field, surface test sites were chosen in granite, limestone and shale rock masses, as well as an underground case study at the Golden Giant Mine. In general, higher capacities were obtained under conditions of higher radial confinement. A correlation between the laboratory and the field test results was obtained through a comparison of the radial stiffness of the laboratory pipes with that of the field boreholes as measured using a high-pressure dilatometer. As the degree of radial confinement increased the failure mechanism changed from radial fracturing and lateral displacement of the grout annulus under low confinement, to shear of the cement flutes and pull out along a cylindrical frictional surface under high confinement.*

---

## INTRODUCTION

Since their introduction into the mining industry over 20 yr ago, fully grouted cable bolts have become one of

the primary support systems for large underground openings. However the success with which they have been used varies considerably. Previous research [1] established that failure most commonly occurred by slip at the cable-grout interface, and that the peak strength is related to frictional rather than adhesional resistance between the steel and the cement. Additional laboratory

---

†Department of Mining Engineering, Queen's University, Kingston, Ontario, Canada K7L 3N6.

tests [1,2] evaluated the importance of operator controlled parameters such as grout quality, rusty vs greasy cables, empty breather tubes and grout tubes, on the ultimate bond capacity of the cable. However a poor correlation between earlier laboratory results and those obtained from comparable short embedment length field tests undermined the use of the former as a practical design tool. Two possible explanations for this discrepancy have been isolated:

(i) differences in the pulling procedures, and in particular the freedom of the embedded cable to rotate during a test (Fig. 1a); and

(ii) differences in the radial confinement of the cable bolt system between laboratory and field as provided by a steel pipe and the rock mass, respectively (Fig. 1b).

In a recent paper, Bawden *et al.* [3] presented a full discussion of the former, while the influence of the latter was indicated by a series of short embedment length cable pull tests conducted by Noranda Technology Centre in a variety of different rock masses [4]. Results from the latter displayed considerable variability, but in general showed higher pull out strengths for better quality, higher stiffness rock masses.

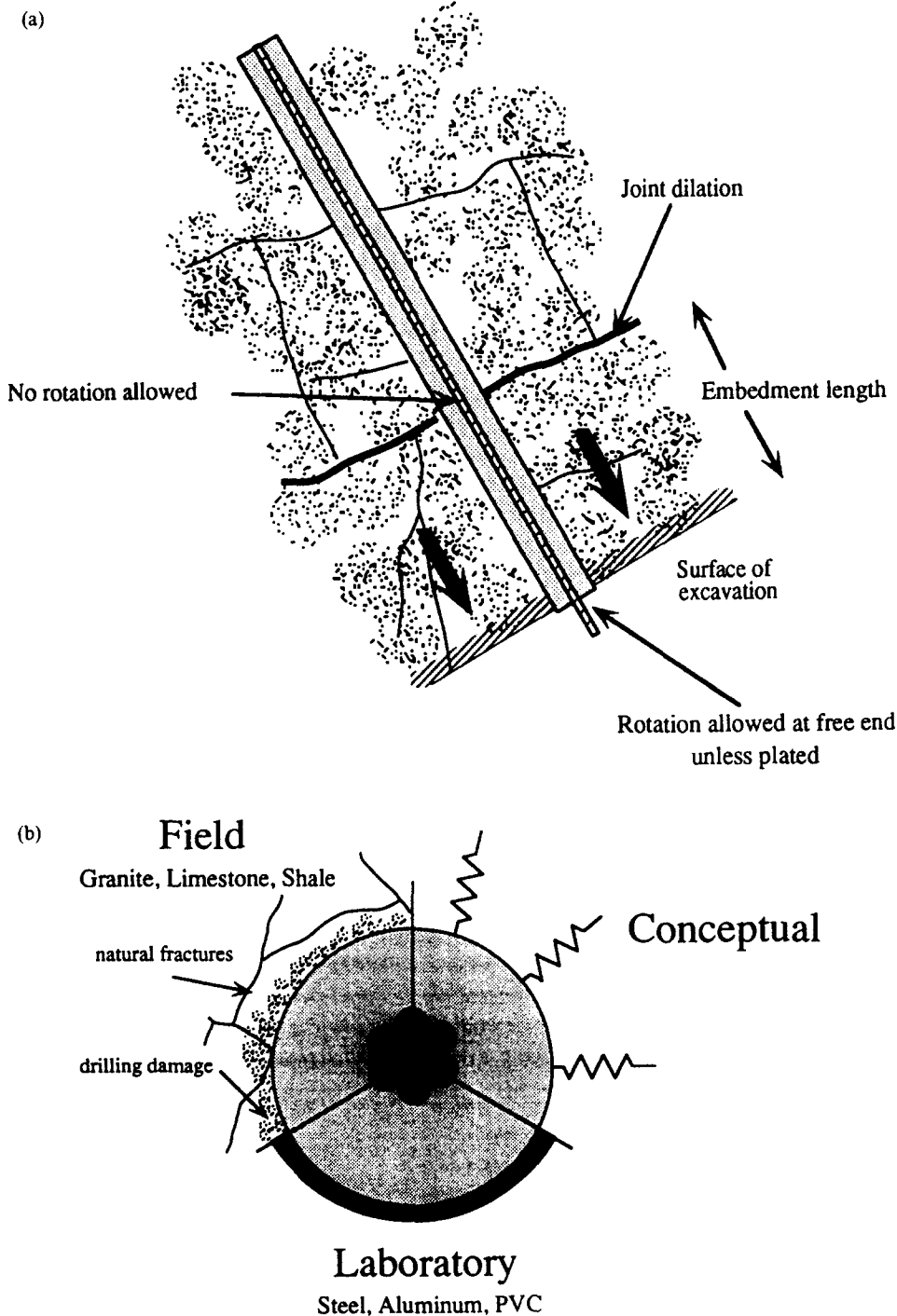


Fig. 1. Key concepts in cable bolt analysis: (a) the concept of embedment length; and (b) boundary conditions to the cable bolt system: conceptually, in the laboratory and in the field.

A test programme was devised to overcome the limitations of previous test procedures, through the elimination of the two inconsistencies listed above, in an attempt to demonstrate a correlation between laboratory and field tests. The results, which form the basis of this paper, have been interpreted in terms of the failure mechanisms observed upon sectioning of specimens after failure. A detailed theoretical consideration of the laboratory results is presented in a related paper [5].

## PROPERTIES OF TYPE 10 PORTLAND CEMENT

### Background

It is a well known fact that in solids there exists an inverse relation between porosity ( $p$ ) and strength ( $S$ ). Strength resides in the solid part of the material hence voids are detrimental to strength. Mehta [6] suggested that this relation is of the form  $S = S_0 e^{-kp}$ , where  $S_0$  is the intrinsic strength of the material (i.e. its strength with zero porosity) and  $k$  is a constant. For a cement paste, the volume of void space depends on the amount of water mixed with the cement at the start of hydration and on the degree of hydration. When the cement sets, it acquires a stable volume that is approximately equal to the original volumes of cement and water.

Rather surprisingly, relatively little recent work has been directed towards determination of the mechanical properties of cement paste (attention has been focussed on concretes, lightweight concretes, fibre-reinforced concretes etc.), especially to the low water:cement ratio grouts that modern pumps are able to produce. Therefore, a comprehensive investigation (see Ref. [7] for complete details) was undertaken in order to determine the physical and mechanical properties for cement grouts with water:cement ratios (by weight) varying between 0.7 and 0.25. Samples were mixed using an MAI (mix and inject) pumping system [8]. They were subsequently left to cure for 28 days at a relative humidity of 95%.

### Structural properties of 28 day cure Portland cement

Figure 2a shows a plot of the variation of void content ( $V_{\text{total}} - V_c$ ) with water content ( $Wc$ ) for a wet cement paste.† Notice the departure from a fully saturated cement paste below a  $Wc$  of 0.5. This effect is reflected

†Water:cement ratio ( $w:c$ ) and water content ( $Wc$ ) are related through the equation:

$$Wc = \frac{1}{1 + \frac{\rho_w}{\rho_c w:c}}$$

where  $\rho_c$  is the density of cement and  $\rho_w$  is the density of water. ‡All UCS and triaxial strength tests were performed on cylindrical samples with a length:width ratio greater than 2, and usually close to 2.5, and at a displacement rate of 0.05 mm/sec. No attempt was made to eliminate frictional effects between the smooth steel platens and the sample. Young's modulus was determined from the stress-strain response of the uniaxial compressive tests between 30 and 60% UCS. Triaxial tests were conducted in a conventional Hoek cell. Tensile strengths were obtained from Brazilian tests.

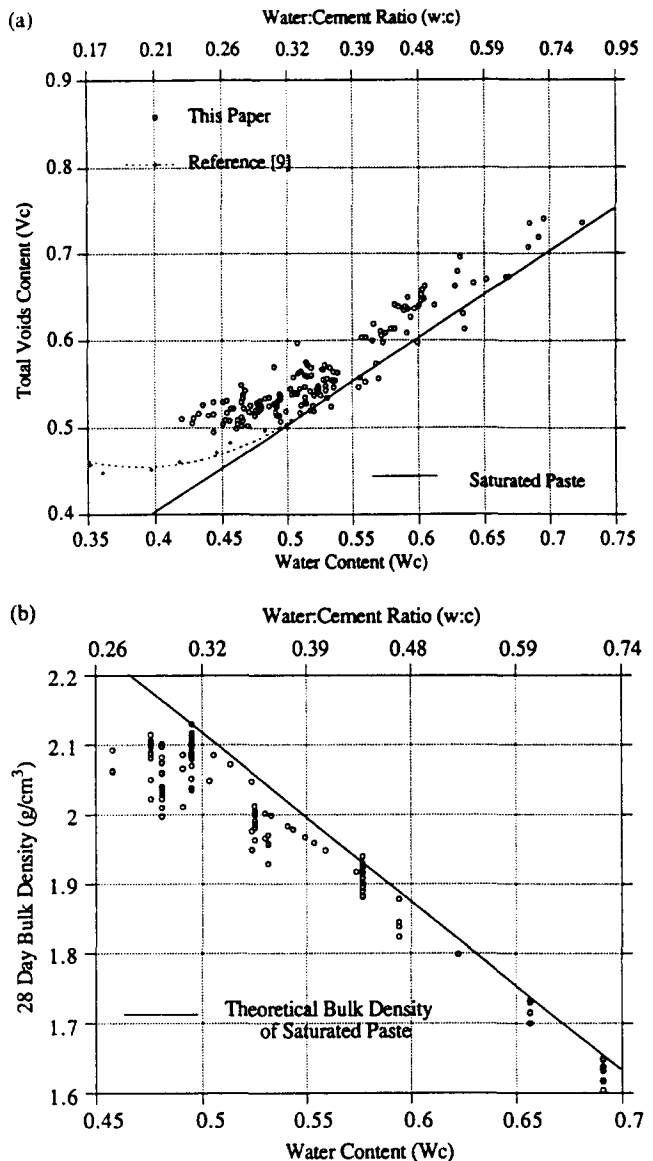


Fig. 2. Physical properties of type 10 Portland cement paste: (a) total voids content ( $V_c = V_{\text{air}} + V_{\text{water}}/V_{\text{total}}$ ) against water content for a wet cement paste. Departure from the line  $V_c = Wc$  indicates air entrapment; and (b) 28-day dry density against water content. The straight line represents the theoretical density of a saturated cement paste assuming  $\rho_{\text{cem}} = 3.15 \text{ g/cm}^3$ .

in the density of the hydrated cement paste (Fig. 2b), and is associated with two phenomena:

- (i) insufficient water is available to saturate the capillary void space between the cement grains; and
- (ii) air pockets (1–3 mm) become entrained within the very thick paste as it flows.

### Mechanical properties of 28 day cure Portland cement

For water:cement ratios ranging from 0.7 to 0.35, the UCS, tensile strength and Young's modulus all increase.‡ The Poisson's ratio remains almost constant (0.18–0.19). However, for water:cement ratios less than 0.35, only the Young's modulus continues to increase as expected (Fig. 3a), while any trend in the strength data is overshadowed by an increase in the scatter of both the UCS (Fig. 3b) and the tensile strength (Fig. 3c) results.

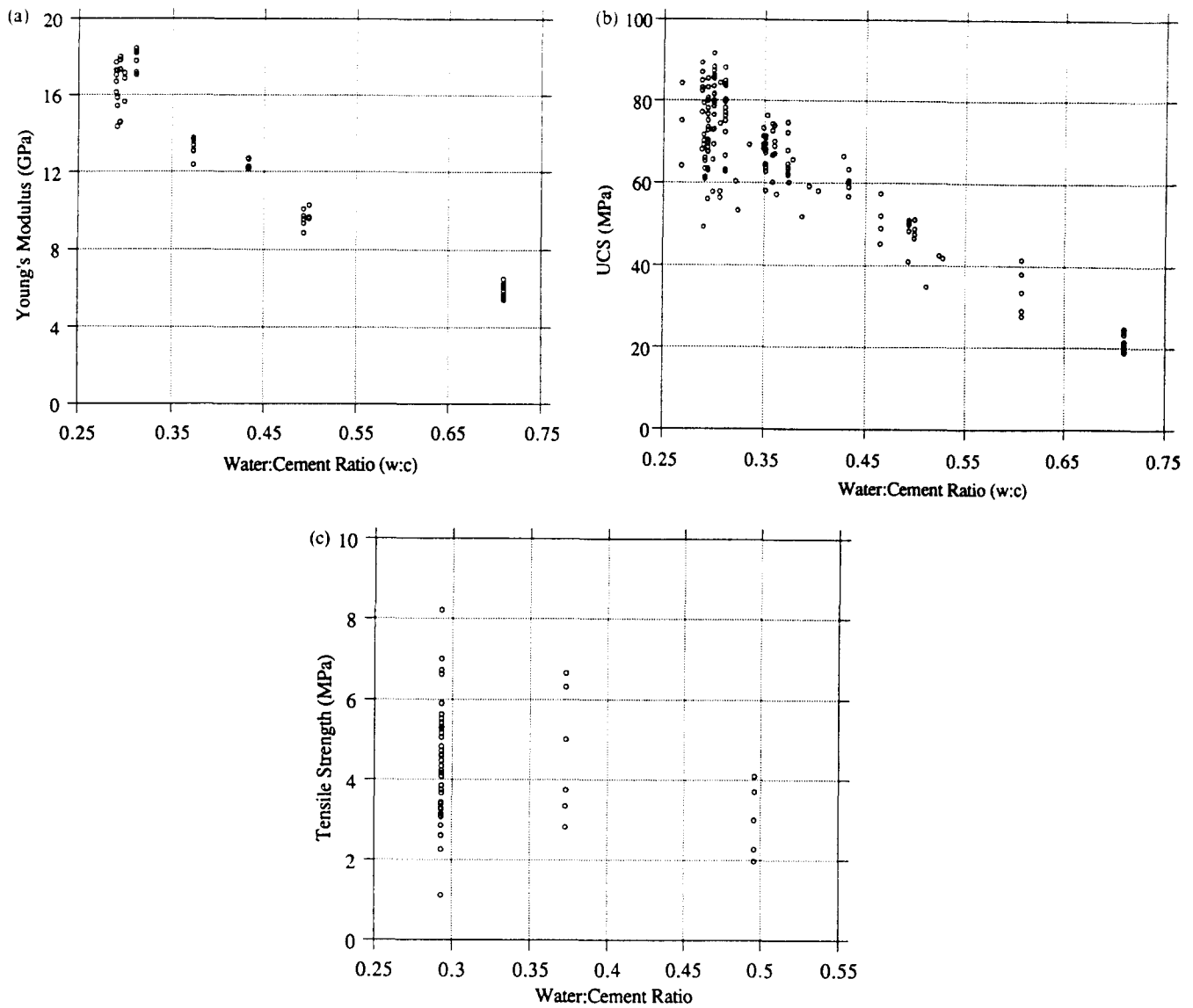


Fig. 3. Mechanical properties of 28-day Portland cement paste: (a) Young's modulus; (b) uniaxial compressive strength; and (c) tensile strength.

This behaviour is related to the structural properties discussed in the preceding paragraph.

The effect of confining pressure on the strength of 0.32, 0.40 and 0.51 water:cement ratio grouts is presented in Fig. 4 and Table 1. The internal coefficients of friction for the peak strength are significantly lower than for rocks. They range from 0.51 (27.0°) for a 0.32 water:cement ratio grout to only 0.36 (20.2°) for a 0.51 water:cement ratio grout. However, the residual strength (strength after 5% axial strain) exhibits a much higher pressure dependency with coefficients ranging from 0.87 (41.0°) to 0.51 (26.9°). A transition from very brittle to

ductile behaviour occurs under relatively low (5–10 MPa) confining pressures. Intuitively, such pressure-dependent behaviour should correlate with that observed from cable pull tests under different degrees of radial confinement.

Although the general trends discussed above may apply to many grout pumping systems, the details are undoubtedly a result of the particular mixing system used rather than being true material properties. However, a qualitative assessment of grouts with various water:cement ratios suggests that grout of 0.3 water:cement may be both impractical and undesirable for cable bolt applications; firstly because it is difficult to

Table 1. Mohr-Coulomb coefficients for the grout for peak and residual strengths: coefficients of friction ( $\mu$ ), angles of friction [ $\phi = \tan(\mu)$ ] and cohesion values for different water:cement ratios. The residual values represent an envelope for the strength of the grout in a fractured state (after 5% axial strain)

w:c ratio	Peak			Residual		
	$\mu$	$\phi$ (degrees)	$\tau_0$ (MPa)	$\mu$	$\phi$ (degrees)	$\tau_0$ (MPa)
0.32	0.51	27.0	18.91	0.87	40.95	3.07
0.40	0.41	22.6	15.55	0.86	40.8	2.39
0.51	0.36	20.18	11.52	0.51	26.9	6.34

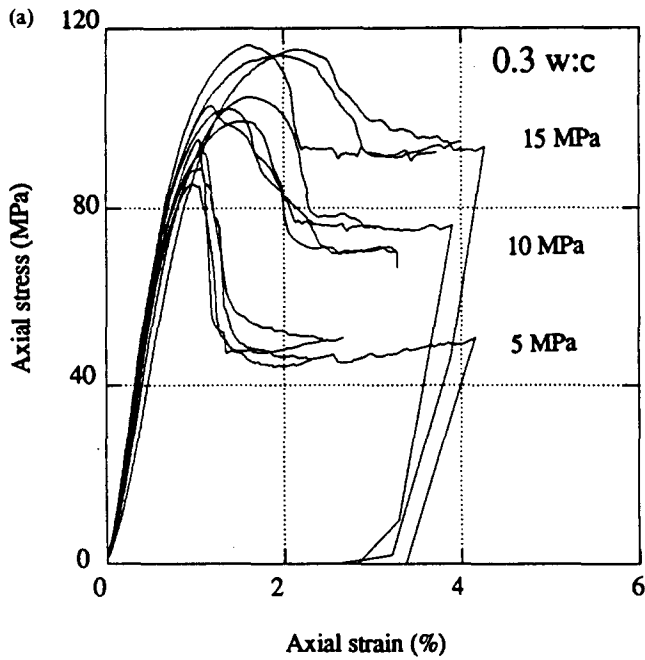


Fig. 4a. The effect of confining pressure on the compressive failure of 0.32 water:cement ratio grouts.

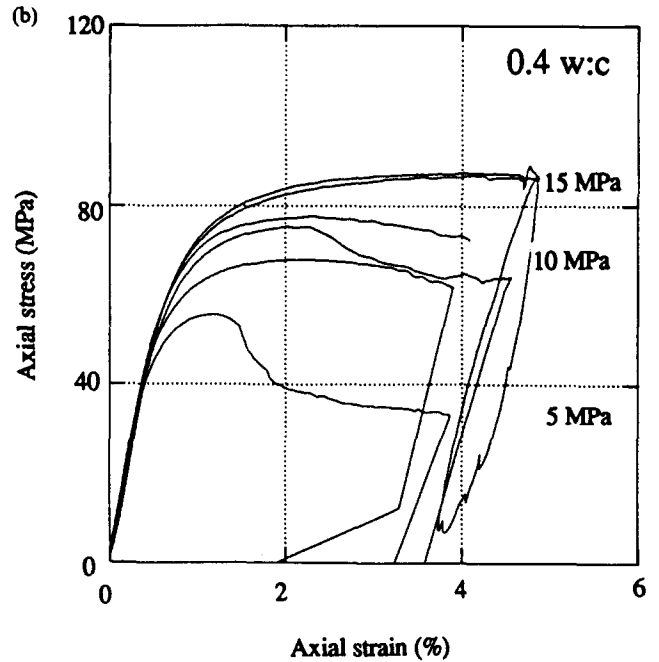


Fig. 4b. The effect of confining pressure on the compressive failure of 0.40 water:cement ratio grouts.

pump, and secondly because of its variability in strength. Instead, slightly thinner grouts with water:cement ratios ranging from 0.35 to 0.40 appear to represent a practical compromise.

**THE PULL TEST PROGRAMME**

The primary objective of the cable bolt pull test programme was to demonstrate a correlation between laboratory and field results for pull tests conducted under varying degrees of radial confinement. The combined scope of the laboratory and field programmes is outlined in Table 2. A standard embedment length of 250 mm was used, so as to be comparable to that used by previous workers.†

Five tests were conducted for each set of parameters. This was assumed to be a minimum representative number, owing to the possibility of losing one due to unforeseen circumstances. Only highly circumspect results have been omitted. The scatter within the results is regarded as an inherent property rather than due experimental error.

*Laboratory Pull Tests*

*Background*

Laboratory experiments conducted by workers in related fields [10-13] have addressed many of the

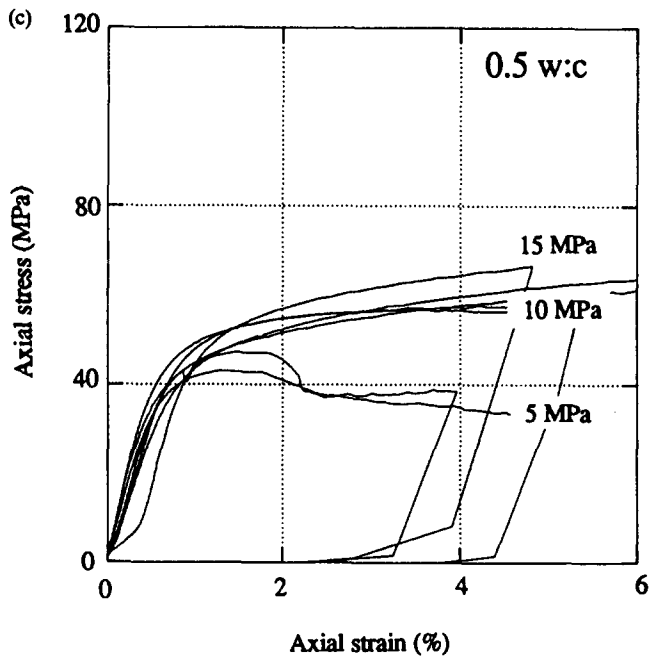


Fig. 4c. The effect of confining pressure on the compressive failure of 0.51 water:cement ratio grouts.

Table 2. The complete pull-test programme

Embedment w:c	250 mm			375 mm 0.3	500 mm 0.3
	0.3	0.4	0.5		
Confinement					
Steel	x	x	x		
Al	x				
PVC	x	x	x		
Granite	x	x	x	x	x
Limestone	x	x	x		x
Shale	x	x	x	x	x
Hemlo HW	x				
Hemlo ore	x				

†For tests on deformed bars the embedment length used is short enough (usually 4-5 times the bar diameter) to ensure a uniform distribution of shear stress, but long enough to reduce the scatter in the test results observed at very short embedment. The philosophy adopted for the selection of embedment lengths for cable pull tests is completely different: embedment lengths are chosen to correspond to typical fracture spacings observed in mining practice (usually 250-300 mm), so that the embedment length is 15-20 times the cable diameter. Consequently, when analyzing the test results, and interpreting failure mechanism, variations in shear stress along the length of the cable cannot be ignored.

fundamental aspects only now being addressed for cable bolts. From pull out tests on deformed bars from concrete, two failure modes have been isolated. One mode involves radial splitting of the concrete cover surrounding the bar, and the other shearing of the reinforcement against the surrounding concrete. Which mechanism dominates depends primarily on the thickness of the cover. The radial splitting mechanism is induced by the wedging action between the lugs of the bar and the concrete. This exerts an outward pressure on the inside of the concrete annulus that is balanced by the induced tensile circumferential stress within the annulus. However, if the tensile strength of the cement is exceeded, radial splitting will occur, the circumferential stress in the concrete annulus will be reduced to zero as will the associated reaction force at the steel-concrete interface, so resulting in failure. The shearing mechanism involves crushing of the concrete ahead of the ribs on the bar, eventually making pull out along a cylindrical frictional surface possible. Bazant and Sener [10] argue that the pull out of reinforcing bars from concrete cubes is profoundly influenced by the brittle character of the two mechanisms described above.

An extensive body of literature exists concerning numerical and analytic analyses of both these failure mechanisms. Within the reinforced concrete literature, the use of short embedment length (less than 5 times the bar diameter) tests has enabled analysis, based on a single cross-sectional slice, of the radial splitting mechanisms [11]. At the other extreme, in the fibre-reinforced concrete literature, pull tests are conducted with embedment lengths 10–100 times the fibre diameter, so that emphasis is on the explanation of progressive non-simultaneous axial debonding [12]; however, for simplicity, the fibres are assumed smooth. Any equivalent analysis of cable pull tests (embedment lengths commonly 15–30 times the cable diameter) requires some combination of the two, a subject of considerable complexity which will be more fully discussed in a forthcoming paper [5].

#### *Laboratory pull test procedure*

Previously all creditable laboratory cable pull tests had been conducted on cables grouted into steel pipes [usually 50.8 mm (2 in.) schedule 80], according to the "split-pipe" test devised by Fuller and Cox [1] (Fig. 5)

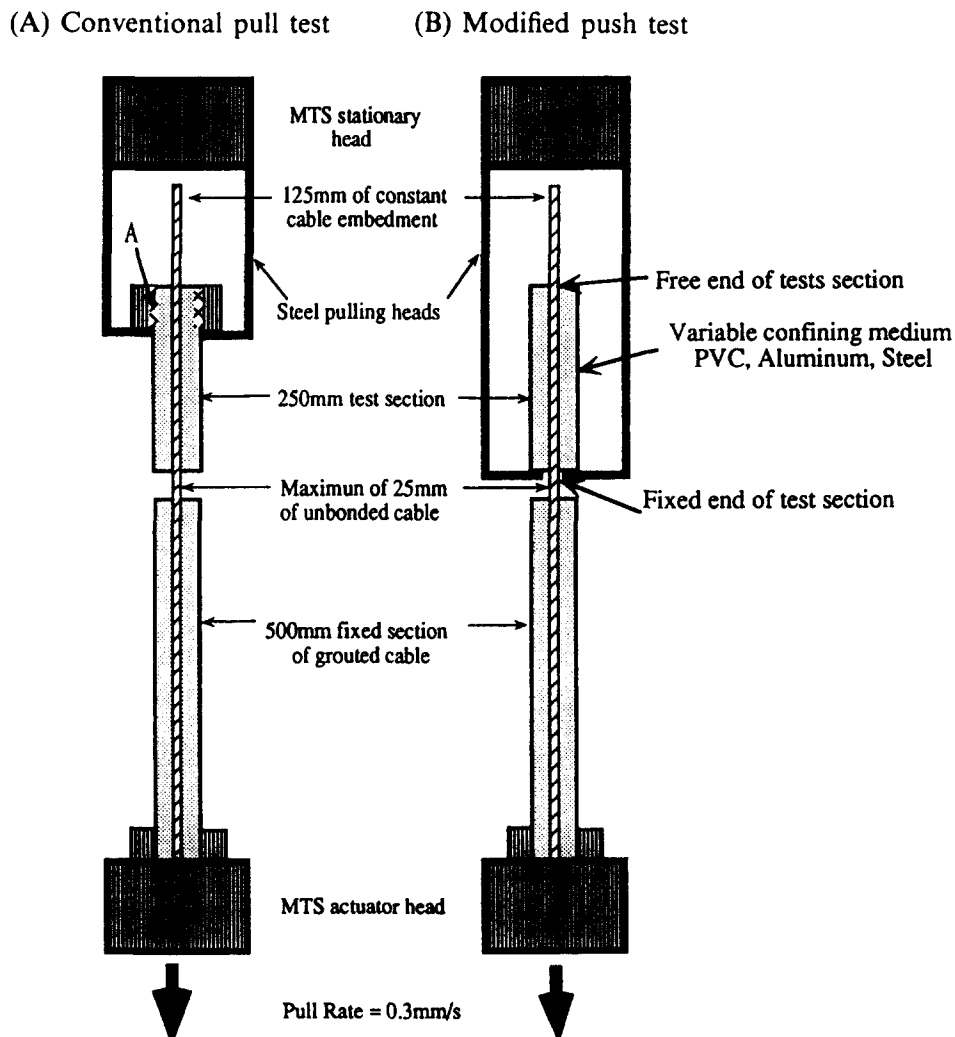


Fig. 5. Comparison between the: (A) conventional pull test; and (B) modified push test. The mining scenario that these experiments intend to reproduce is shown in Fig. 1a.

Table 3. Radial wall stiffness of the confining pipes used for the laboratory pull tests

	$E$ (GPa)	$\nu$	$d_o$ (mm)	$d_i$ (mm)	$K_r$ (MPa/mm)
Steel	200	0.25	60.13	49.30	1604.2
Al	72	0.25	60.45	49.02	599.5
PVC	3	0.32	60.61	47.50	37.7

or some variation of it. However, in order to enable testing under different radial confinements, the current programme used Al and PVC as well as steel pipe. In addition, and primarily for visual purposes, tests were also conducted in a thin transparent heatshrink sleeve that provided negligible radial confinement. This necessitated a modification of the conventional test procedure as shown in Fig. 5, so that in essence the grout column and confining pipe are "pushed" rather than "pulled" off the cable. A comparison between both methods (see Ref. [8] for details) indicated no significant difference between the two test methods.† During a test, force may be applied to both the lower surface of the grout annulus and the bottom edge of the confining pipe, so that care must be taken in analyzing the initial stiffness of the tests. Obviously both procedures do not entirely conform to the field scenario of a block of rock sliding off a cable, but the modified push test procedure does overcome the potential for excess confinement in the vicinity of the pulling threads that can occur in the conventional pull test (point A, in Fig. 5).

The radial stiffness ( $K_r$ ) of the pipes used for confinement can be calculated from thick wall cylinder theory according to the equation:

$$K_r = \frac{2E}{(1 + \nu)} \left\{ \frac{d_o^2 - d_i^2}{d_i [(1 - 2\nu)d_i^2 + d_o^2]} \right\}, \quad (1)$$

†It is interesting to note that within the fibre-reinforced concrete literature, "push" tests are the standard method of "pull" testing a fibre from concrete (see Ref. [12], p. 154).

where  $E$  and  $\nu$  are the Young's modulus and Poisson's ratio for the material comprising the pipe ( $E = 3$  GPa and  $\nu = 0.32$  for PVC,  $E = 71$  GPa and  $\nu = 0.25$  for Al and for  $E = 196$  GPa and  $\nu = 0.25$  for steel), and  $d_i$  and  $d_o$  are the inside and outside diameters of the pipe, respectively. Appropriate values of  $K_r$  are listed in Table 3.

Rotation was *prevented* at all points except the free end of the cable, and all tests were conducted at a constant pull rate of 0.3 mm/sec.

#### Laboratory pull test results

Figure 6 shows the load-displacement curves for each confining material in laboratory tests with 0.30

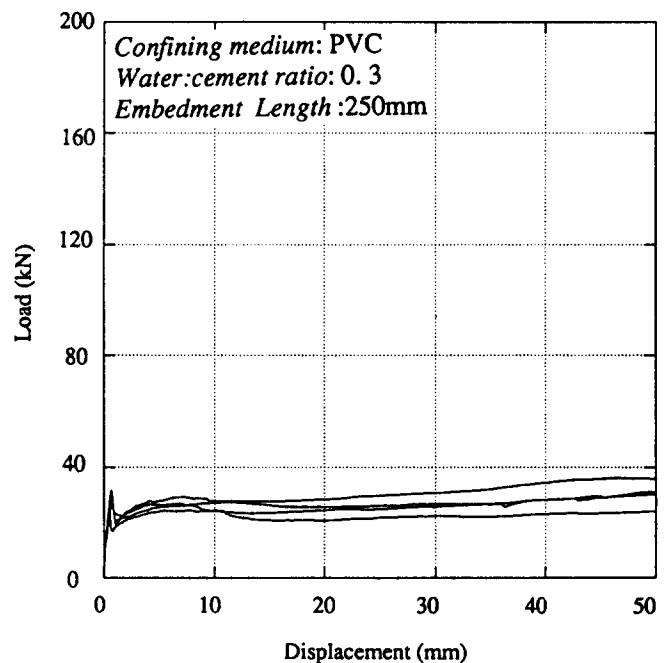
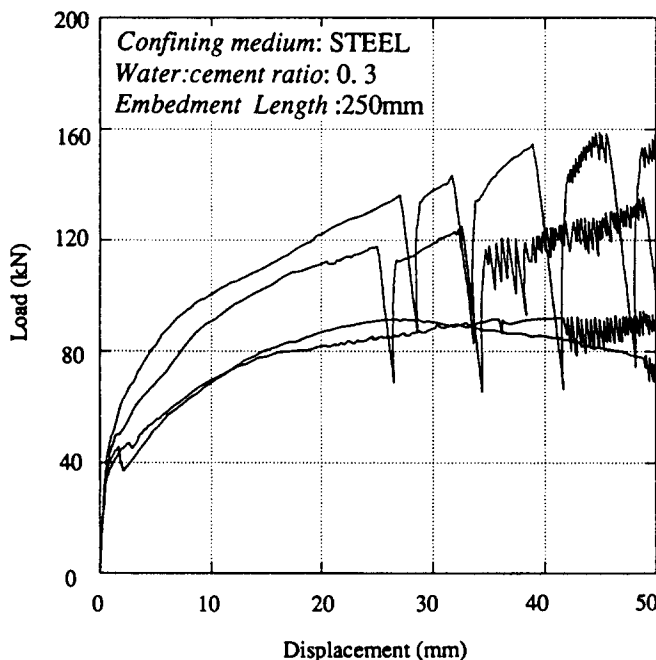
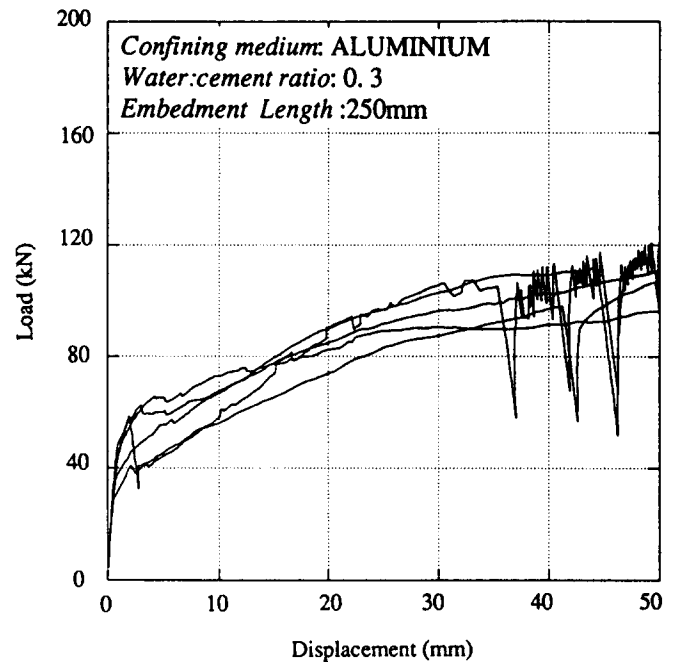


Fig. 6a—Caption opposite.

Fig. 6a. Laboratory pull test results for a 0.3 water:cement ratio grout.

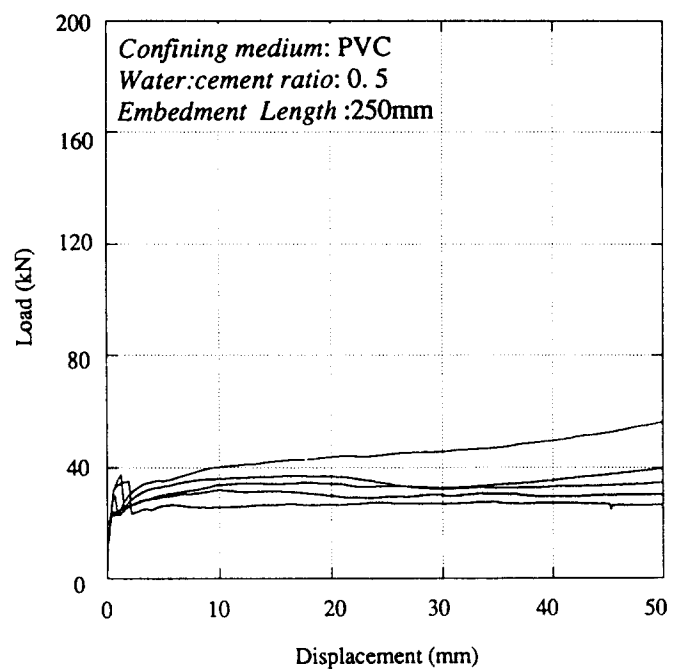
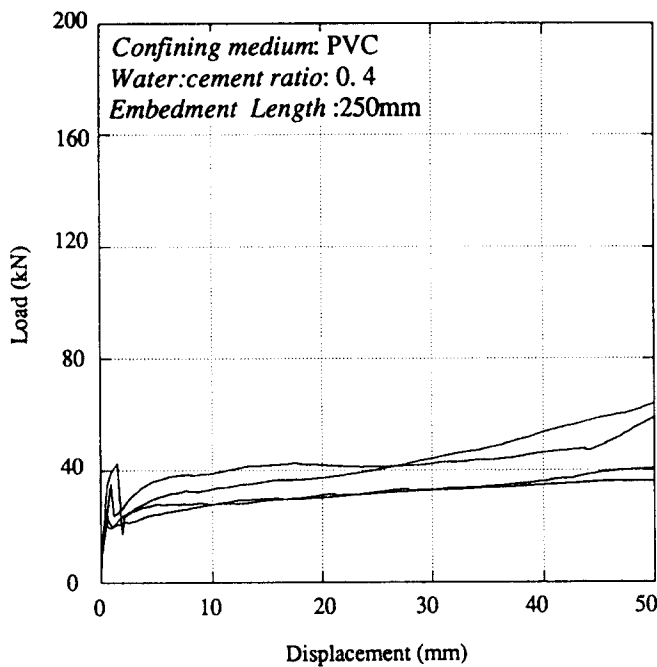
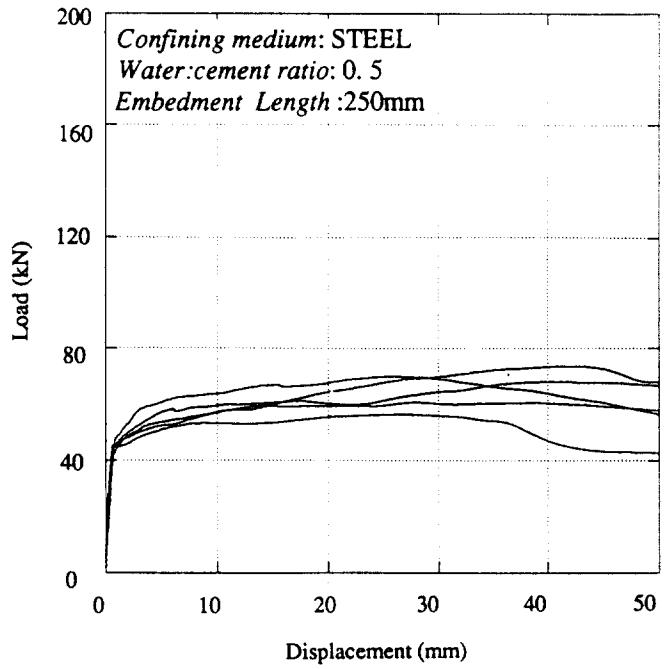
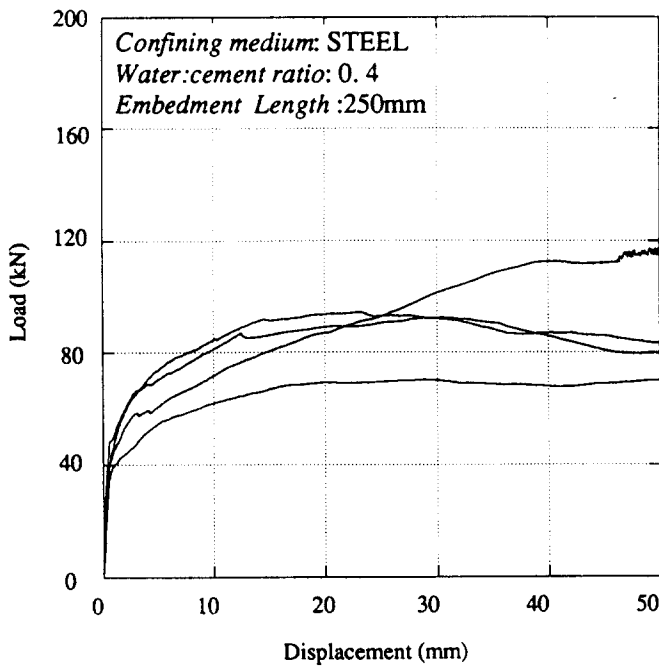


Fig. 6b. Laboratory pull test results for a 0.4 water:cement ratio grout.

Fig. 6c. Laboratory pull test results for a 0.5 water:cement ratio grout.

(UCS = 78 MPa), 0.40 (63 MPa) and 0.50 (48 MPa) water:cement grouts. The results show the strong influence of radial confinement on the ultimate cable bolt capacity, and in particular the effect that low water:cement ratio grouts have in emphasizing this effect. Although the highest strengths were obtained from the 0.3 water:cement ratio grout the scatter was also high, particularly at high confinements. This may correspond to the scatter in the strengths of low water:cement ratio grouts ( $< 0.35$ ) discussed previously (refer back to Fig. 3b and c).

Bawden *et al.* [14] suggested that the load-displacement plots could be divided into definite stages,

each associated with a specific failure mechanism as cable bolt failure proceeds. Specimens that had reached various stages of failure were sectioned for both visual and SEM analysis. Further tests were conducted with subminiature pressure transducers inserted into the grout annulus [5]. Based on these results, Fig. 7 shows schematically the distributions of shear stress ( $\tau$ ) at the cable-grout interface, the axial stress in the cable ( $\sigma$ ) and also the dominant failure mechanism as pull out progresses.

*Stage 1.* The essentially linear response that characterizes the initial stage of a pull test is related to the axial stiffness of the cable, the elastic properties of the grout

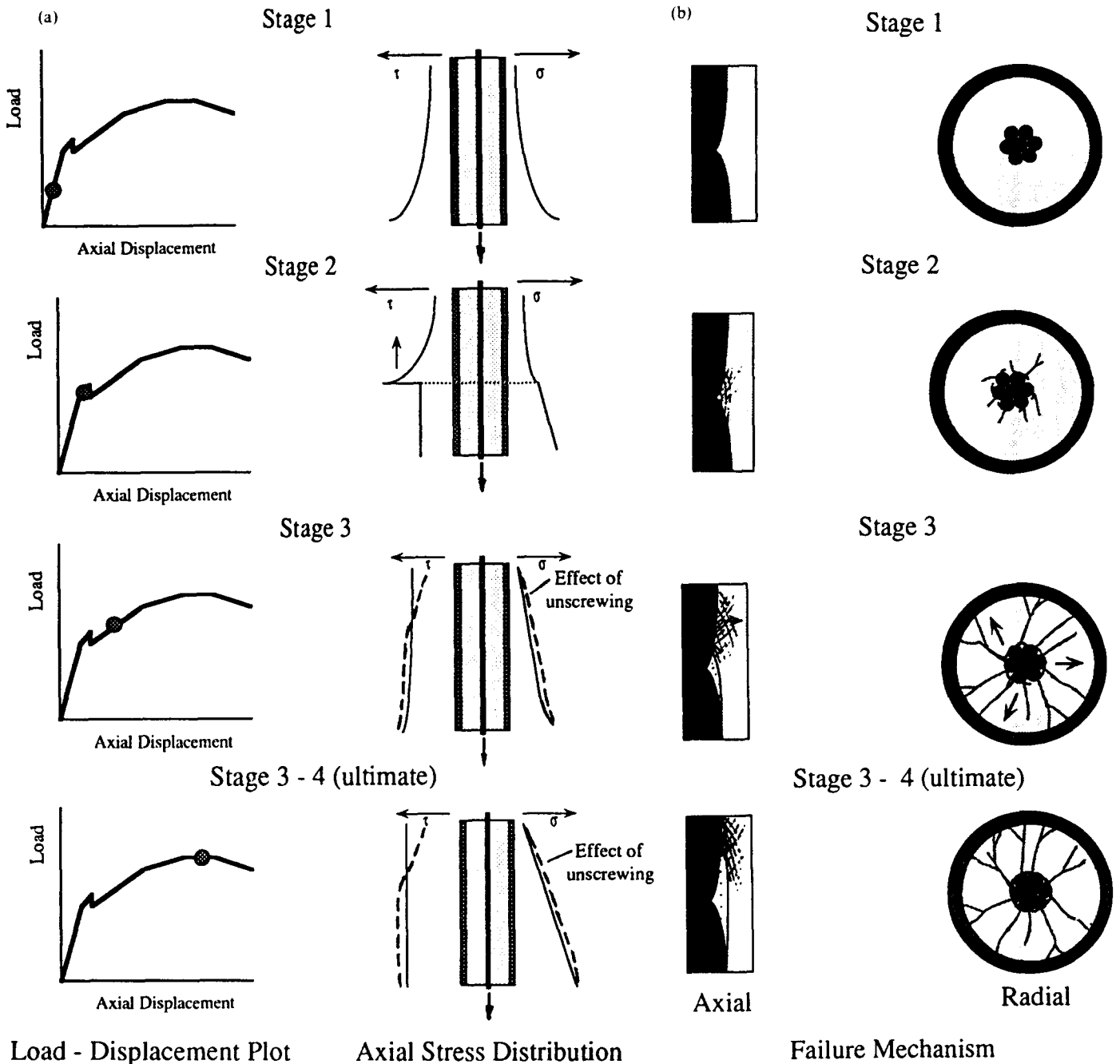


Fig. 7. Successive stages in the failure during a pull test: (a) the stress distribution along the cable; and (b) the failure mechanism for a single flute and a section perpendicular to the axis of the cable.

and the properties of the interface between the two. It is usually assumed that the interface comprises an adhesional bond. However, experiments involving the pull out of single, smooth, straight wires [1, 5] from a cement paste, indicate that the initial stiffness is significantly less (by a factor of 3–5) than that predicted from appropriate elastic solutions: either analytic [15] or numerical [1]†. A similar discrepancy exists between the initial stiffness for pull tests on 7-strand cables and elastic analytic solutions [15] that assume the

cable can be represented by a 5/8" (15.9 mm) bar with an equivalent axial modulus of 140 GPa.‡ Two explanations for this discrepancy are:

- Any steel–cement composite is characterized by a "transition zone" at the interface between the two, wherein the microstructure of the current paste is considerably different from that of the bulk paste away from the interface [6, 12]. In this region the cement paste is much more porous due to bleeding and entrapment of water along the surface of the steel, and irregular packing of the cement grains within a zone 20–40  $\mu\text{m}$  from the interface.
- The adhesional bond between the steel and the cement is not continuous but instead comprises a

†Fuller and Cox were able to obtain a correspondence between their experimental results and results from a finite element model, but only by assuming that the Young's modulus for the grout was 660 MPa or approximately an order of magnitude less than determined from the test.

‡From tests by manufacturer, Stelco Inc.

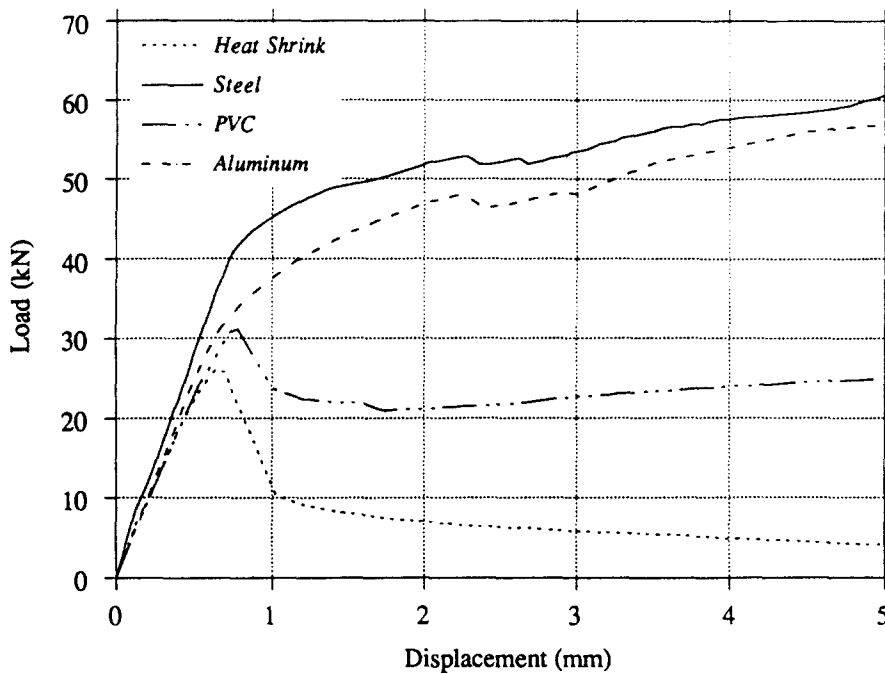


Fig. 8. Typical load-displacement curves for pull tests in different confining media at displacements up to 5 mm.

series of point contacts, resulting in a relatively weak and compliant bond.

These phenomena are further reflected in the low shear and tensile strengths of steel-cement interfaces. Shear tests by Lutz and Gergely [16] gave a shear strength of between 1.93 and 4.13 MPa, and tests by Aydan *et al.* [17] indicated even lower values; 1.2–1.5 MPa. Furthermore, results are very sensitive to the surface finish (i.e. rusty, greasy etc.). These values are almost an order of magnitude less than the shear strength of cement paste.

Consequently, the bond between steel and cement, which is associated with the initial linear response during a pull test, although partially adhesional probably involves additional components related to:

- (i) the mechanical interlock the cement and cable and the bearing capacity that this provides; and
- (ii) frictional resistance related to radial compression induced by shrinkage of the grout annulus during curing.

*Stage 2.* Even though the bond at the cement steel interface is relatively weak, only limited slip can occur unless either:

- (i) radial fracturing of the grout annulus breaks it into distinct wedges, which can then be radially displaced to allow sliding at the cement-steel interface; or
- (ii) shear failure through the grout flutes occurs.

The initiation of one or both of these mechanisms is responsible for the reduction in axial stiffness during

*Stage 2.* Figure 8 indicates that the onset of non-linearity is dependent on the confining medium, occurring at higher loads for higher confinement. As discussed by Hyett *et al.* [5], from theoretical calculation, the initiation of both mechanisms should be dependent on the radial confining pressure, so that this observation in itself does not specify which is responsible for the reduction in axial stiffness observed at the beginning of *Stage 2*.

During *Stage 2* both mechanisms are stable. Figure 8 indicates that for tests conducted in steel and Al confining pipes axial displacements upwards of 2 mm are attained, prior to instability. However, for tests conducted in PVC and heatshrink one or both mechanisms are immediately unstable, and in fact one probably acts to trigger the other, resulting in a very brittle mode of failure.

The stress drop occurring at the end of *Stage 2* may correspond to either:

- (i) Unstable propagation of radial fractures through the remainder of the grout annulus, which will result in a decrease in radial compression at the grout-cable interface, and hence an instantaneous reduction in the frictional resistance to pull out; or
- (ii) Unstable shear failure of the grout flutes along the remaining length of the cable, which will reduce their strength from peak to residual values.

For steel and Al, the observation that this stress drop occurs at relatively high displacement ( $> 2$  mm) suggests that it is related to the radial fracturing mechanism. As shown in Fig. 8, the maximum loads obtained during *Stage 2* for Al and steel are 40–50 kN. The cable has an axial stiffness of 0.009 mm/kN over a 250 mm length, and so stretch of the cable can only account for at most 0.40–0.45 mm of displacement.† The remainder, 1.5–1.55 mm, must be associated with shear of the grout

†This is an upper bound because the axial load in the cable decreases along its length.

flutes. Such displacements are well beyond those expected for flutes at peak load.

**Stage 3.** In general, the load attained during Stage 3 is controlled by a combination of:

- (i) the frictional resistance to sliding at the steel-cement interface; and
- (ii) the residual strength of the cement flutes (Fig. 7).

Both phenomena are pressure sensitive. First, the coefficient of friction for sliding along a smooth cement-steel interface is approx. 0.6 [12]. Second, as shown in Table 1, the coefficient of internal friction for the residual strength of cement (i.e. its strength in the fractured state) ranges from 0.87 (0.32 water:cement ratio) to 0.51 (0.51 water:cement ratio).

As cable displacement increases, the radial confining pressure on which the frictional resistance to cable pull out, is controlled by the potential for greater geometric mismatch between the cable and cement flutes. How far the individual wedges that now comprise the grout annulus can be pushed aside is determined by the radial stiffness of the confining medium (Fig. 1a). When the radial stiffness is low (i.e. for a compliant rock mass) the favourable failure mechanism is lateral displacement of the wedges: when it is higher, dilation is suppressed and failure is more likely to occur by shear of the grout flutes and pull out along a cylindrical frictional surface. Much higher radial compression, and hence a much higher frictional resistance to pull out is mobilized in the latter case [5]. These mechanisms represent end-members, and in reality some combination of the two usually operates.

Except for the heatshrink experiments, the peak strength during cable pull out is achieved after considerable axial displacements (40–50 mm) and therefore it is the response during Stage 3 that principally determines the ultimate cable bolt capacity. Figure 9 shows the load attained at the end of the three stages designated above (i.e. at the transition between Stage 1 and 2, between Stage 2 and 3 etc.) for the different confining media. The effect of the confinement medium is most significant during Stage 3.

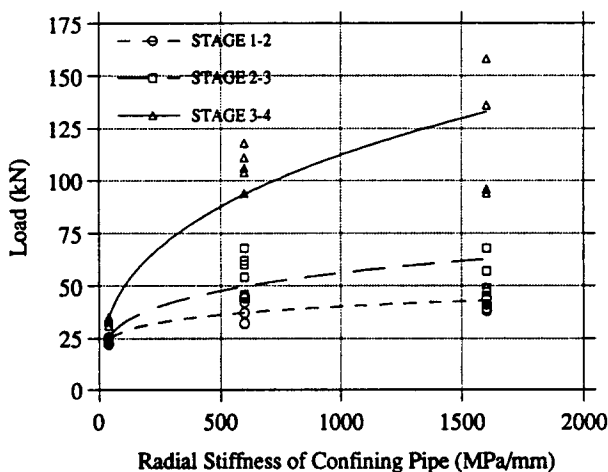


Fig. 9. The loads attained at critical points during pull tests in different confining media. The effect of different confining media is greatest during Stage 3 (i.e. between the Stage 2–3 transition and the Stage 3–4 transition or ultimate load).

**Stage 4.** The ultimate cable bolt capacity is usually attained after 40 or 50 mm of displacement, at which point (in the absence of cable twist) the geometric mismatch between the cable and grout flutes is a maximum (Fig. 7). A subsequent decrease in capacity may result from:

- (i) a negative dilation angle as the grout flute passes its point of maximum mismatch and begins to interlock into the next “cusp” along the cable; and
- (ii) continued fracturing of the grout flutes,

or, of course, some combination of the two.

#### Role of the cable “unscrewing” mechanism

Based on microscopic examination of failed samples, the failure mechanism, as described above, is always characteristic of the grout annulus at the fixed end of the test section. However, due to low torsional rigidity of the cable, and depending on the embedment length, the free end is able to rotate relative to the fixed end (see Fig. 5) so enabling failure to occur there by an “unscrewing” rather than shear mechanism. This contention is supported by the observation that damage to the grout flutes decreases towards the free end of the test section (especially for higher radial confinements), and in some cases the flutes there remain completely intact. Pull tests for which the entire test section was free to rotate (see Ref. [3], Fig. 1) result in significantly lower pull out strengths. This must be reflected in the load distribution along the cable, particularly during Stages 3 and 4 of the pull out process (see Fig. 7), with the fixed end (shearing mechanism) supporting a higher proportion of the load than the free end (unscrewing mechanism).

The foregoing discussion has outlined the failure mechanisms observed during cable pull tests with emphasis on the role that radial confinement plays. The intention throughout the remainder of this paper is to demonstrate that the laboratory results presented above can be correlated with *in situ* cable pull tests based on a correlation of radial confinement, and hence that they have some relevance to the design of fully grouted cable bolt systems in underground engineering practice.

#### FIELD PULL TEST PROGRAMME

As discussed above, the correlation between laboratory and field cable pull test results depends on finding practical solutions to two problems: first, how to determine the radial stiffness of the cable bolt hole wall; and second, how to eliminate rotation during the pull test.

Three field locations were selected at surface localities within the Kingston area. The first two were quarries within shale and limestone, the third was a surface outcrop in granite gneiss (Fig. 10). Tests were conducted in 59 mm (2.25”) percussion holes which were vertical and 2 m deep. A further series of pull tests were conducted 546 m underground at the Golden Giant

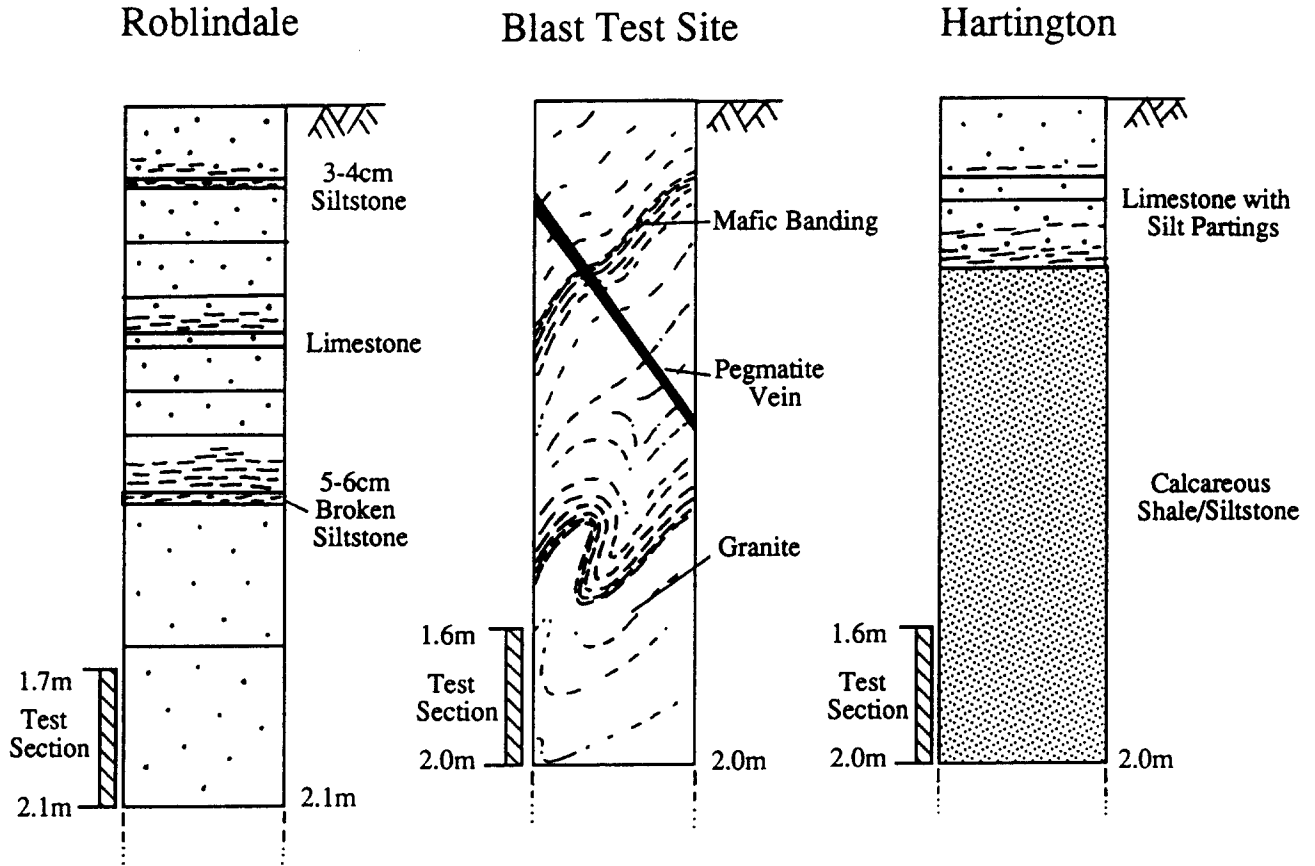


Fig. 10. Geology at the tree surface locations in the Kingston area (Roblindale quarry is in limestone, the blast test site is in granite and Hartington quarry is in shale).

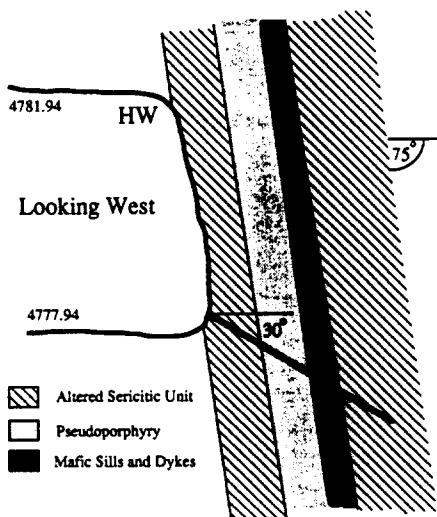
Mine (Fig. 11). In this case 63 mm (2.5") inclined holes were used. The full scope of the field programme is outlined in the lower part of Table 2.

*Determination of the radial stiffness of the borehole wall*

A high-pressure dilatometer (HPD) was used to determine the radial stiffness of the cable bolt holes. The instrument is a high-pressure (0–25 MPa), direct

strain measurement, hydraulically inflated packer comprising six strain gauge arms arranged for the measurement of radial deformation across three axes aligned at 120° to one another. All calibrations and corrections were conducted in accordance with the ISRM suggested method [18] for the use of a flexible dilatometer with radial displacement measurement. The instrument is designed to operate in 76 mm diamond drill holes, the

(a) HEMLO GOLDEN GIANT MINE  
4775 Level



(b) HEMLO - GOLDEN GIANT MINE  
4775 level

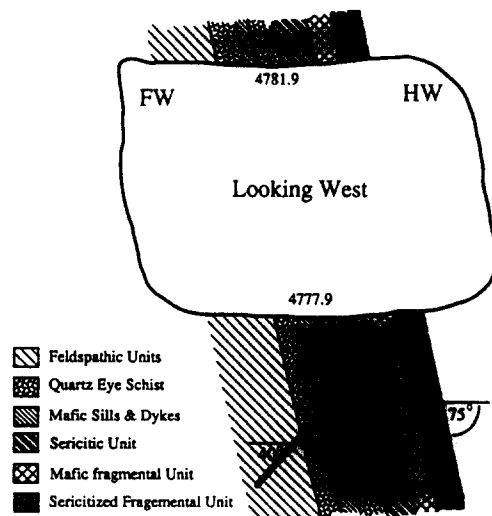


Fig. 11. Geology at the Golden Giant Mine in: (a) the hanging wall; and (b) the ore.

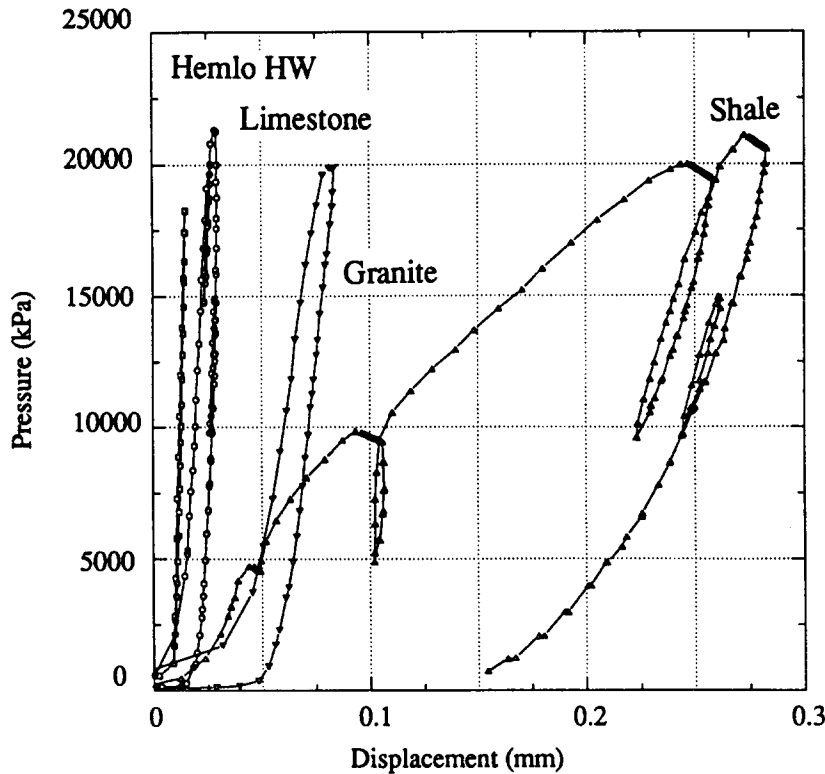


Fig. 12. High-pressure dilatometer-radial deformation response for the three surface sites and the hanging wall at Golden Giant.

radial stiffness of which can be related to the stiffness of the 57 mm (2.25 in.) cable bolt holes ( $K_c$ ) through the equation:

$$K_c = \frac{d_d}{d_c} K_d, \quad (2)$$

where  $K_d$  is the stiffness of the dilatometer hole,  $d_d$  is the diameter of the dilatometer hole (i.e. 76 mm) and  $d_c$  the diameter of the cable bolt hole.

At each of the three surface locations there was a tendency for fractures intersecting the 70 cm test section to be jacked open, which usually resulted in splitting of the flexible membrane. In fact the problem was so costly that the number of load cycles conducted for each test section was minimized. In contrast, this problem has never occurred during underground testing, despite the fact that fractures are known to have intersected the test section.

Pressure-radial displacement responses for the three surface localities and the Hemlo hanging wall are shown in Fig. 12. Individual measurements were taken at 10 sec intervals, and the loading rate was approx. 100 kPa/sec. The results shown were taken immediately following a pre-load cycle (0–10,000 kPa) to seat the instrument.

Lower radial displacements were induced for tests in Hemlo ore and the determination of a representative radial stiffness was judged to be beyond the limit of resolution of the instrument using the current

operating practices. For calibrations on steel pipes in the laboratory this suggests a radial stiffness beyond 1600 MPa/mm. For all three surface localities the response was non-linear below 5000 kPa. Time-dependent deformations were only important for the shale.

Although the radial pressures at wall of the cable bolt hole will increase during a cable pull test, suggesting that the radial stiffness should be determined from the loading paths in Fig. 12, a more reliable estimate of the rock mass response is obtained from the unloading path.† Consequently, radial stiffnesses were determined from the unloading path between 10,000 and 5000 kPa (Table 4) as will be discussed below. Perhaps the most significant result is the difference in borehole radial stiffness between the surface and underground tests.

#### Field pull test procedure

Until recently [3], no coherent set of guidelines or suggested methods exist for the field testing of

Table 4. Radial wall stiffnesses of the cable bolt holes for the field tests based on the high pressure dilatometer results

Rock type	$d_d$ (mm)	$d_c$ (mm)	$K_r$ (MPa/mm)		
			Dilatometer hole	Cable bolt hole	
Granite	76	57	Hole 1	476.2	634.9
			Hole 2	270.2	348.0
			Hole 3	645.2	831.1
Limestone	76	57	Hole 1	657.9	847.5
			Hole 2	628.7	809.8
Shale	76	57	Hole 1	78.7	101.4
			Hole 2	93.6	120.6
Hemlo HW	76	63	1461.0	1754.8	
Hemlo ore	76	63	>1600	>1920	

†From laboratory calibrations it has been determined that during loading slip between the borehole wall, the steel "lantern" surrounding the membrane and the membrane itself can effect the response.

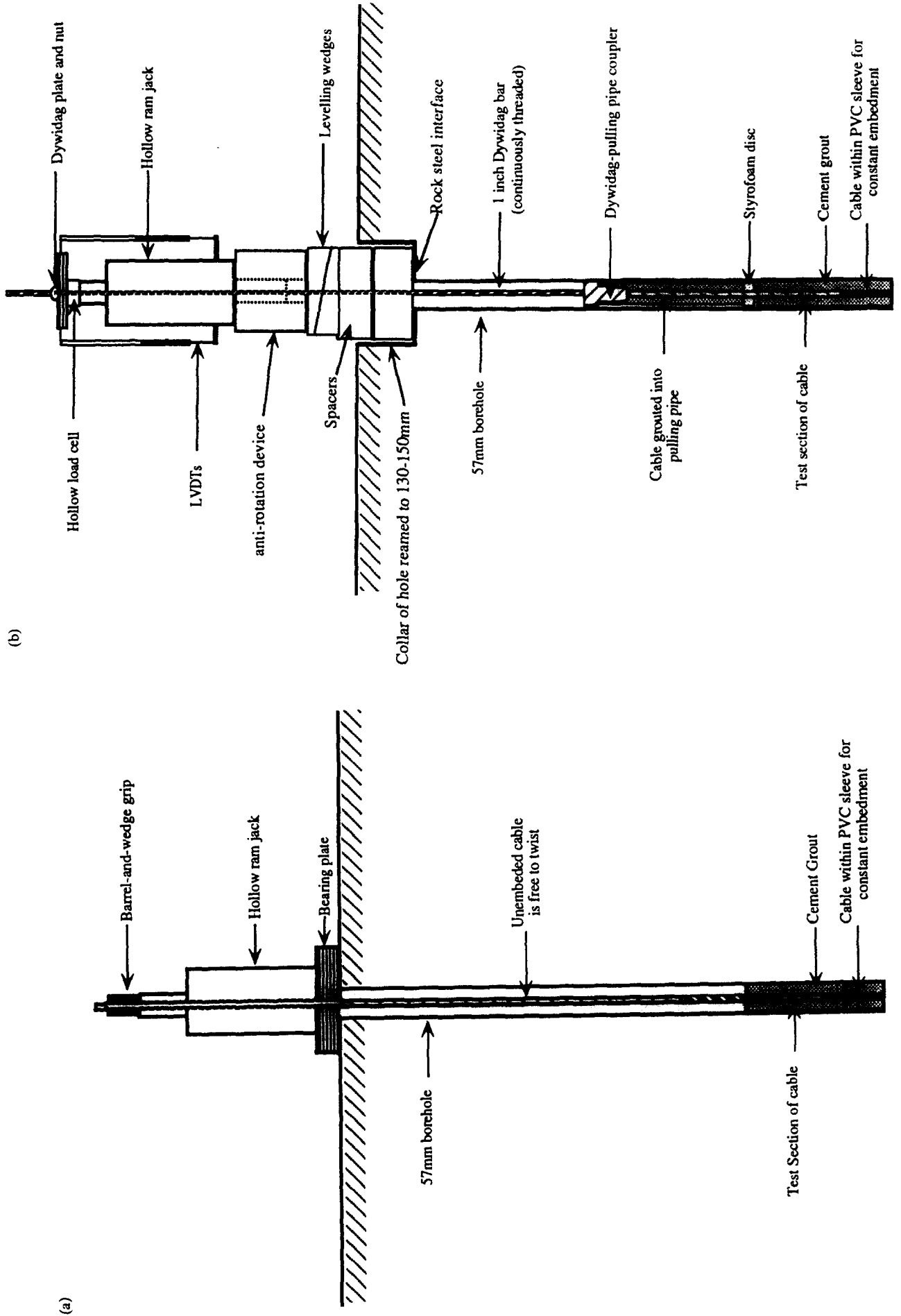


Fig. 13. Field pull test setups: (a) the previously used procedure which does not prevent rotation; and (b) the setup outlined in Ref. [3] which prevents rotation during pulling.

cable bolts. Previous tests involved grouting a short embedment length of cable (usually 250–375 mm) some distance down a borehole, and, as shown in Fig. 13a, pulling on the cable using a barrel-and-wedge grip. This conformed well with the ISRM suggested method [19] for testing rock bolts. However, owing to the low torsional rigidity of the free cable above the test section, rotation is allowed at both ends of the embedded section of cable, enabling failure to occur by an unrealistic “unscrewing” mechanism. In order to overcome this, the pull test setup illustrated in Fig. 13b was devised. The similarity with the split-pipe laboratory test (Fig. 5)

is immediately obvious. Comparative *in situ* pull test results indicate that when rotation is prevented cable capacities increase between 200 and 300% (see Ref. [3]). This helps explain to a large extent the anomalously low field test results obtained by some previous workers. All *in situ* tests were conducted at an average pull rate of 0.3 mm/sec.

#### Field pull test results

Figures 14 shows the load–displacement response for pull tests at the three surface localities. The effect of each test parameter will be discussed in turn.

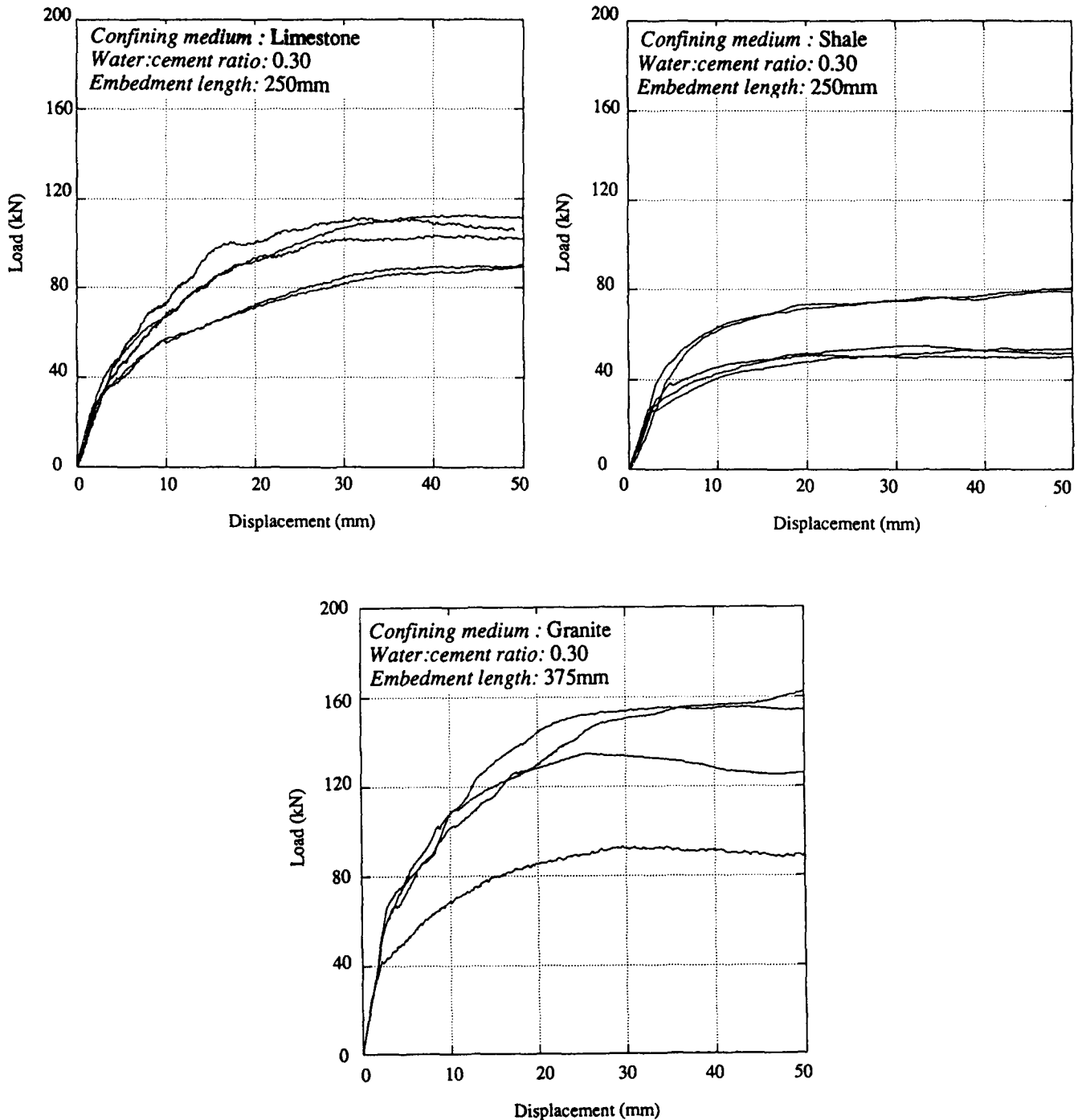


Fig. 14a. Field pull test results for 0.3 water:cement ratio grout.

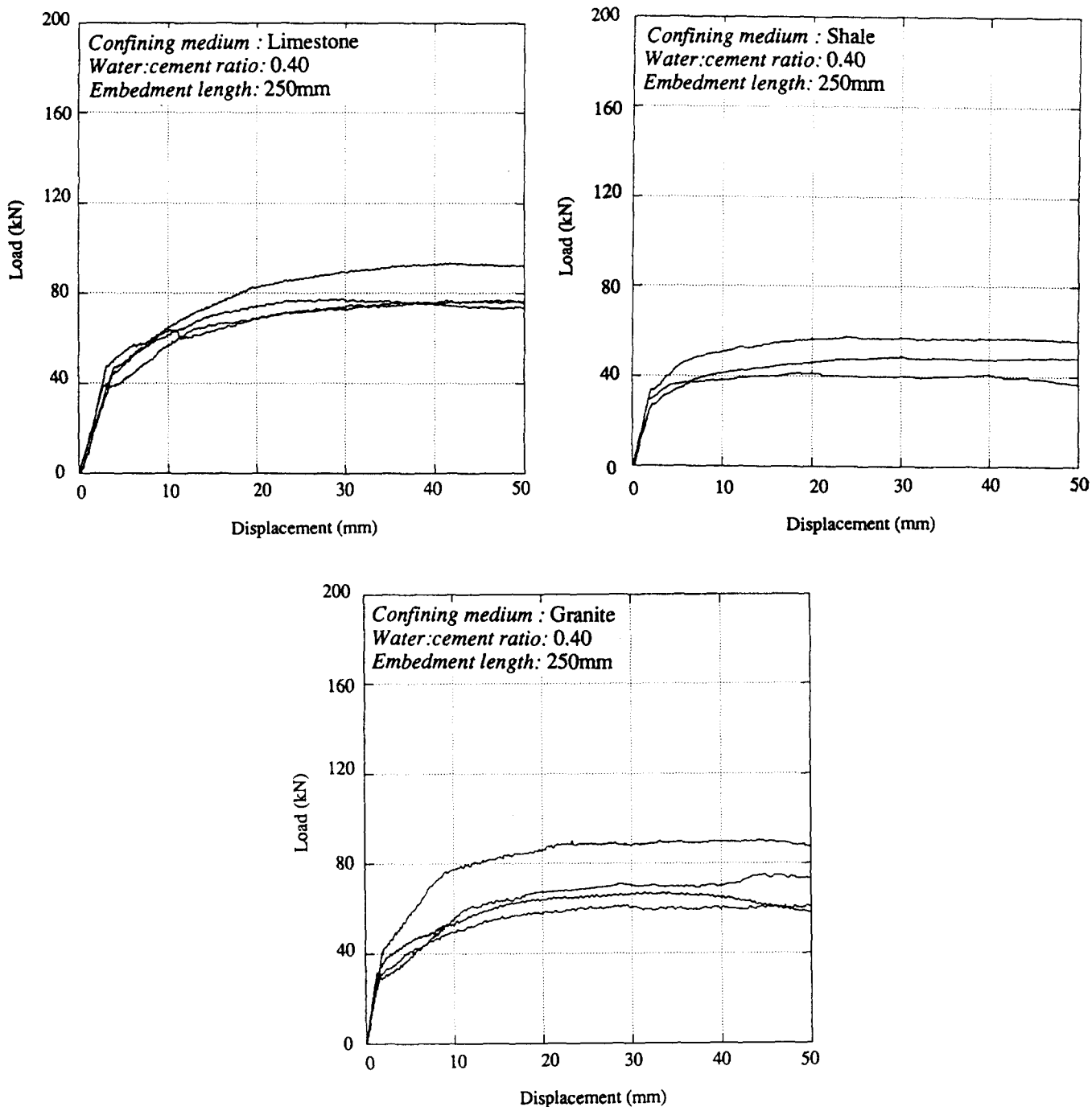


Fig. 14b. Field pull test results for 0.4 water:cement ratio grout.

#### Effect of cement

Pull test results showing the effect of the water:cement ratio for granite, limestone and shale are shown in Fig. 14a-c (upper plots). For both the limestone and granite a 50-75% increase in ultimate cable bolt capacity was obtained in going from a water:cement ratio of 0.50-0.30. For shale the corresponding increase is considerably less.

#### Effect of the rock mass

Figure 14a shows pull test results for each of the surface localities at a 0.3 water:cement ratio.

Similar cable bolt capacities were obtained in the granite and limestone and lower results in the shale. Throughout the test programme the results for the tests in limestone are considerably more consistent than those in either shale or granite. Testing in the limestone was confined to a single massive unit with relatively few natural fractures ( $Q' = 18.7$ ), and as outlined above (Table 5), the dilatometer test results for limestone were very much more consistent than for granite. The effect of confinement was considerably more marked for the lower water:cement ratio grouts.

*Effect of embedment length*

With respect to the tests at different embedment lengths, although cable bolt capacity increased almost linearly over the range of embedment lengths tested, the two were not *directly* proportional (Fig. 15). If peak load was simply due to frictional sliding (i.e. failure that could be described as perfectly plastic), then changes in embedment length and changes in peak load should be proportional (limit analysis concept). However, as discussed above, several aspects of cable bolt failure mechanism are decidedly brittle in nature: in other words

they exhibit a post-peak load decrease. Consequently the failure along the cable is non-simultaneous, with one cross-section having already failed as another further along is approaching peak capacity.

From a practical perspective, the common practice of normalizing cable bolt capacities to load per unit length (usually kN/m or tonnes/m), should be avoided. For instance if a 250 mm pull test achieves an ultimate capacity of 60 kN, then the same cable within a rock mass with a joint spacing of 1 m, may have an ultimate capacity considerably less than 240 kN: how much less will depend on the radial rock mass confinement.

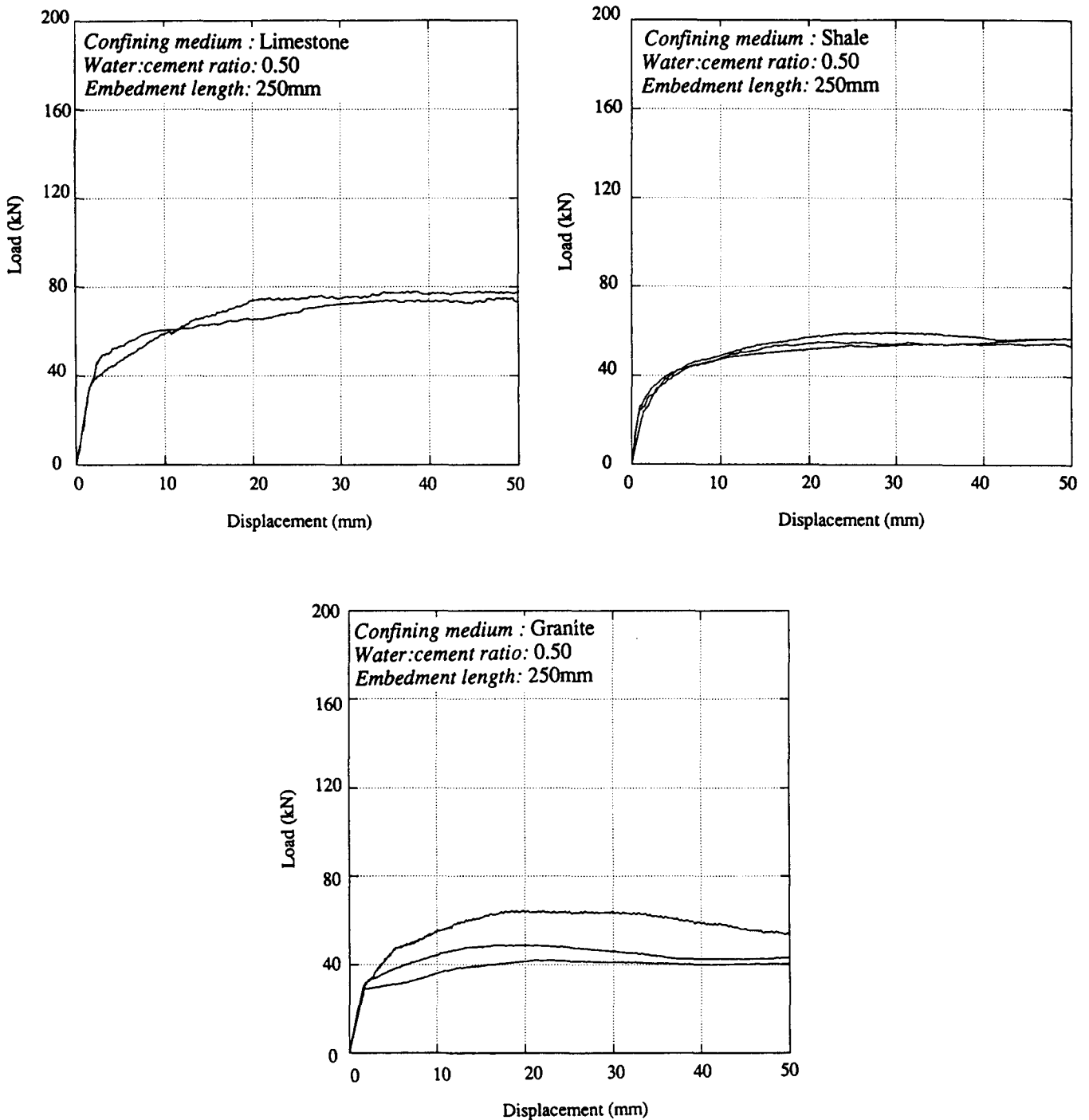


Fig. 14c. Field pull test results for 0.5 water:cement ratio grout.

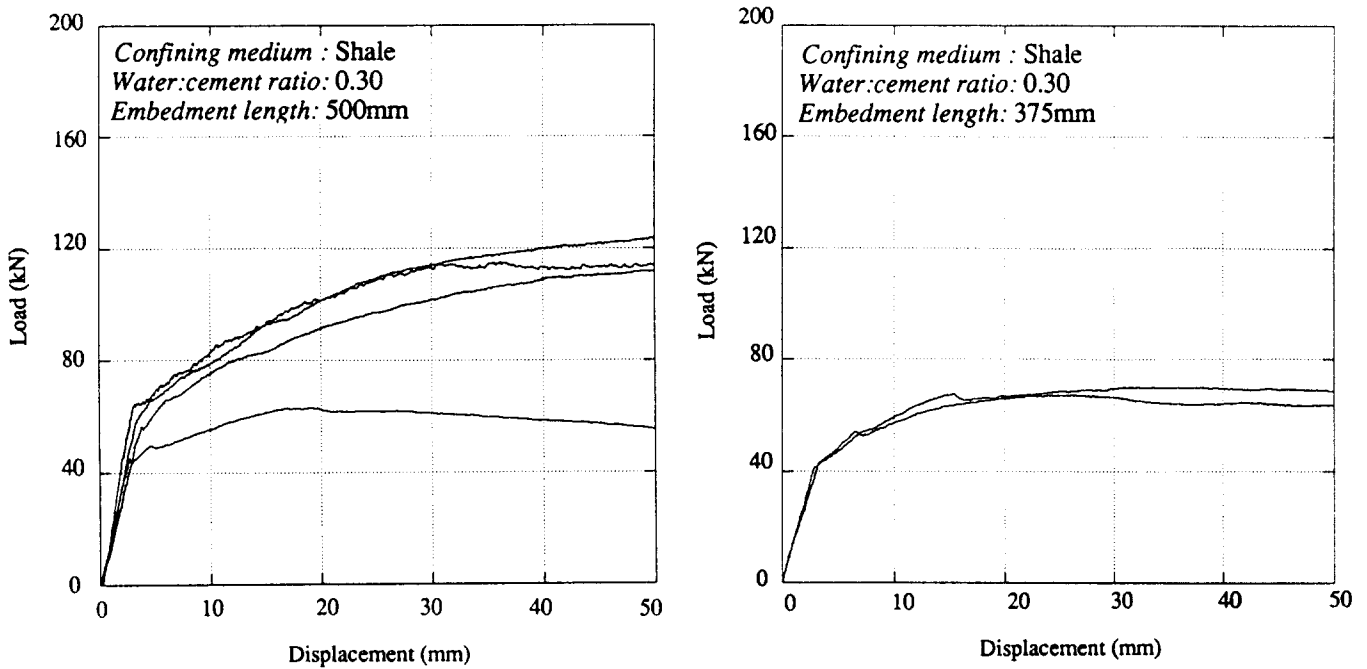


Fig. 14d. Results of tests conducted at different embedment lengths in granite.

*The Hemlo case study*

Figure 16 shows the load–displacement response for tests conducted underground at Hemlo. The tests were conducted on the 4775 level at a depth of 546 m, and well away from any current mining activity.

**COUPLING OF LABORATORY AND FIELD PULL TEST RESULTS**

The coupling of laboratory and field results requires a comparison of the radial confinement provided by

the steel, Al and PVC pipes in the laboratory with the different rock masses in the field. Figure 17 plots the ultimate cable bolt capacity against the radial confinement stiffness for grouts of 0.30, 0.40 and 0.50 water:cement ratio. When the radial stiffness of the confinement is accounted for, a good correlation exists between laboratory and field test results. The effect of radial confinement is most evident for high strength grouts (0.30 and 0.40, UCS > 65 MPa).

Although all previous field test results had to be discarded due to inconsistencies in the pull test

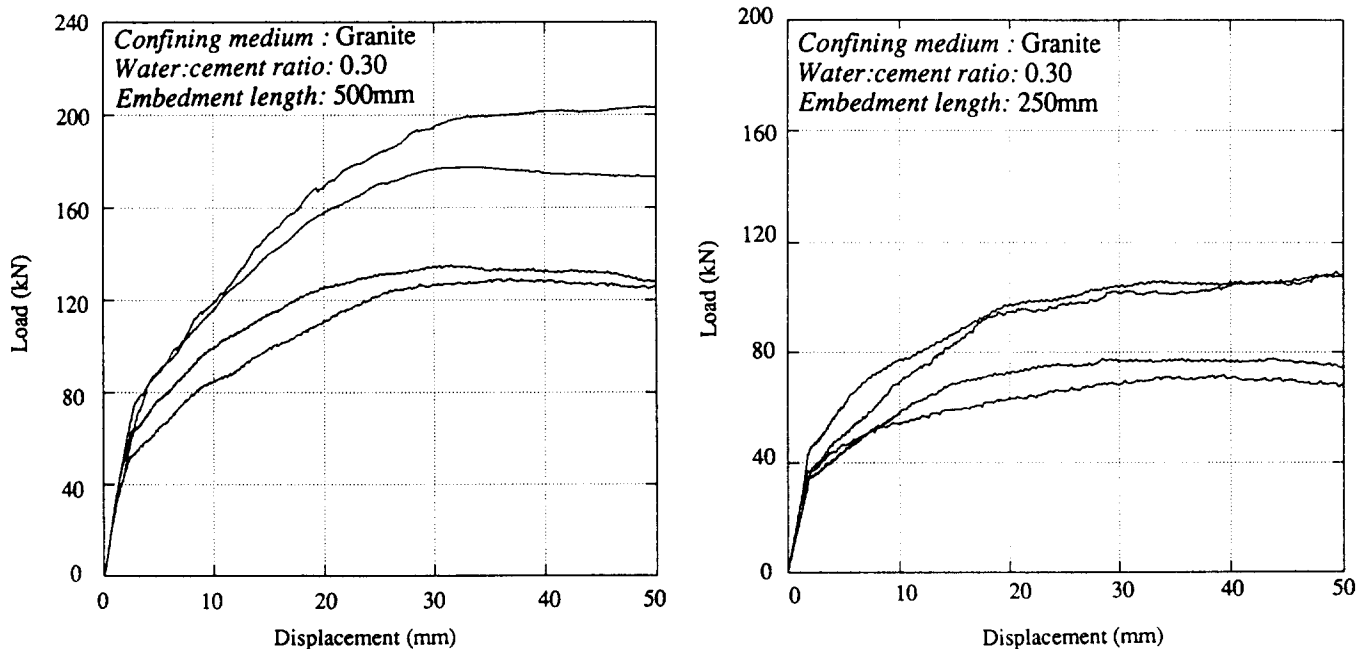


Fig. 14e. Results of tests conducted at different embedment lengths in shale.

Table 5. Rock mass moduli obtained from three different procedures: (i) laboratory tests on core; (ii) from a determination of Barton's  $Q'$ ; and (iii) from the high pressure dilatometer ( $\nu = \nu_{intact}$ )

Rock type	$E_{Intact}$	$E_{Rock\ mass}(Q')$	$E_{Dilatometer}$
Granite	68.6	23.3 (10.0)	22.0
Limestone	62.8	32.3 (18.7)	30.5
Shale	11.5	13.5 (3.5)	4.1
Hemlo HW	54.8	22.3 (9.1)	66.6
Hemlo ore	64.2	26.8 (13.5)	> 68.4

procedure, comparable laboratory data is available from previous research [1, 2]. These tests have been conducted at a range of different embedment lengths. Figure 18 incorporates the influence of embedment length into the correlation and plots data from Refs [1] and [2] together with the results presented in this paper for 0.3 and 0.45–0.5 water:cement ratio grouts. The ultimate cable capacities are indicated on the graph for each set of tests at a given embedment length and radial confinement. Contouring of these values enables the cable capacity to be estimated for any combination of embedment length and radial stiffness. The heavy lines in Fig. 18 show the combinations of embedment lengths and radial stiffnesses for which yield of the cable should occur, for 0.30 and 0.45–0.50 water:cement ratio grouts (insufficient data is available to construct the curve for a 0.40 water:cement ratio grout). The curves have been obtained by extrapolating the linear relations between load and embedment length (presented in Fig. 15 and in Ref. [2]), up to 24 tonnes. The embedment length for which yield of the steel (i.e. optimum design) is expected is 1448 mm for shale, 767 mm for granite and 553 mm for steel, for a 0.3 water:cement ratio grout, and 978 mm for steel with a 0.45 water:cement ratio [2]. Notice that for a 0.45–0.50 water:cement ratio grout the strength

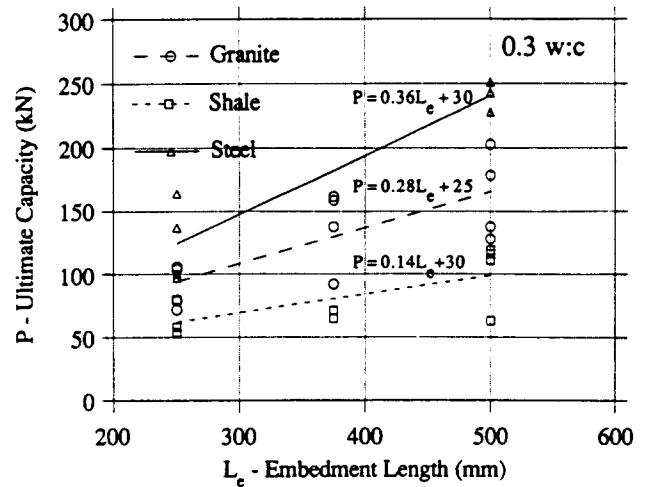


Fig. 15. Peak cable bolt capacity vs embedment length for a 0.3 water:cement ratio grout.

is almost independent of the radial stiffness of the confining medium.

DISCUSSION AND CONCLUSIONS

Application to mining practice

Traditionally cable bolt design has been based on the implicit assumption that the full capacity of the steel cable (normally taken as yield at 24 tonnes or 240 kN) would be mobilized. This contradicted observations of steel cables hanging from failed stope backs and hanging walls that had obviously supported much lower loads. In many circumstances the cables were undeformed, in others they were partially unravelled, but only in very few cases did cables exhibit "pig-tailing" (indicating the cable had reached yield) or actual rupture. The results presented in this paper clearly demonstrate that cable loads approaching the yield strength of the steel cable

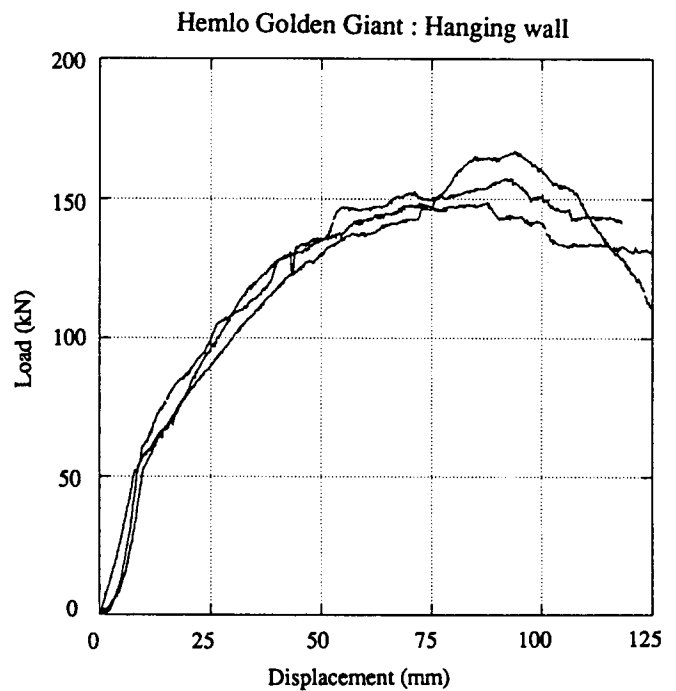
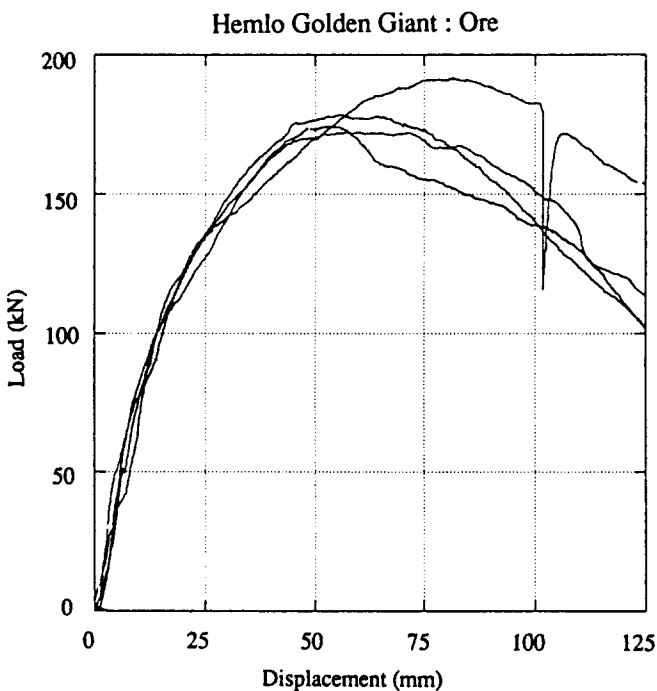


Fig. 16. Pull test results from the Golden Giant case study.

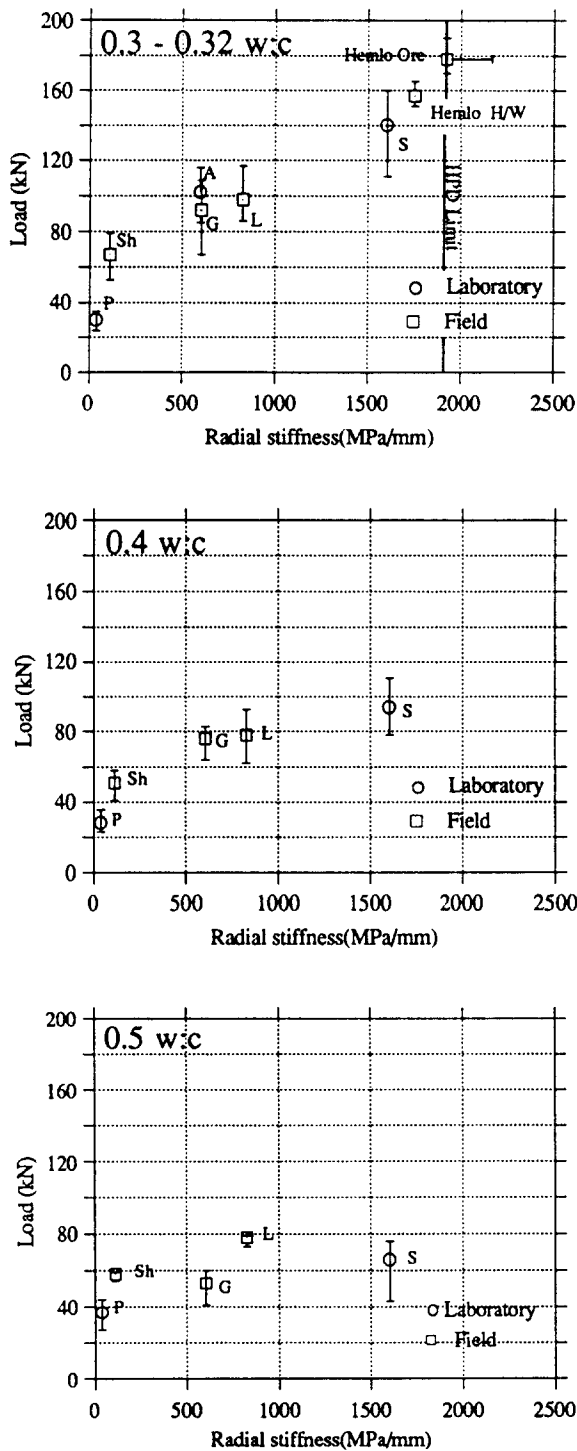


Fig. 17. Comparison of laboratory and field cable bolt capacities accounting for radial stiffness. P = PVC, A = aluminum, S = steel, Sh = shale, G = granite, L = limestone, H/W hanging wall.

can only be mobilized under very specific conditions. Assuming satisfactory cable bolt installation, these involve a combination of:

- long embedment lengths, and
- high radial confinement.

For practical applications, the embedment length and radial stiffness of the cable bolt holes represent geotechnical parameters that are defined by the rock mass. The following discussion provides guidelines on how to obtain them.

*Embedment length*

As indicated in Fig. 1a, the embedment length for a cable is determined by the joint spacing along the axis of cable bolt. In cases where the drill core is available in the appropriate direction a direct estimate of the embedment length can be made based the joint frequency obtained from an RQD. However, care must be taken. Throughout the preceding discussion it has been assumed that cable bolts will be loaded by joint opening perpendicular to the cable axis. In practice, cable bolts may often be subjected to a component of shear, due to either, slip across joints or cables aligned obliquely to joints which are opening. It is generally accepted that shear loading reduces cable capacity (P. Fuller, Personal communication).

*Radial stiffness of cable bolt holes*

The critical influence of the radial stiffness at the wall of cable bolt holes in controlling cable bolt capacity has been outlined above. Many mine operators will not have access to a high-pressure dilatometer, such as the one used in this research, and hence will require guidelines to make an estimate of the radial stiffness at the wall of cable bolt holes. In the general case, this can be done

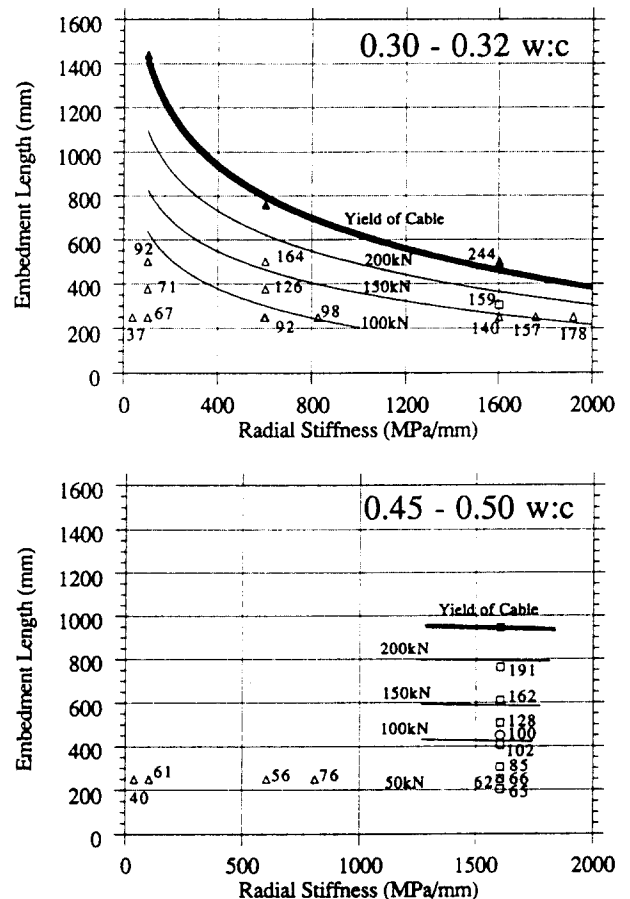


Fig. 18. Effect of both embedment length and radial borehole wall stiffness on ultimate cable bolt capacity for a 0.3 and 0.45-0.50 water:cement ratio grouts. Triangles = this paper, squares = [2], circles = [1]. The number next to the symbol is the peak load from a test at the appropriate confining pressure and embedment length, and the capacities have been contoured. Insufficient data is available to construct the plot for a 0.4 water:cement ratio grout.

using the equation:

$$K_r = \frac{2E'}{(1 + \nu')d_c} \tag{3}$$

where  $d_c$  is the diameter of the cable bolt hole and  $E'$  and  $\nu'$  are representative elastic parameters for the material comprising the borehole wall. Selection of values for  $E'$  and  $\nu'$  must be done carefully. In most circumstances, the intact elastic rock properties will represent upper bounds to these values, whereas the rock mass values obtained from either Barton's  $Q'$  or Bienawski's RMR ratings according to the equation:

$$E_{m} = 10^{(RMR - 10)/40} = 10^{(9 \ln Q' + 34)/40} \tag{4}$$

where  $E_m$  is the rock mass modulus in GPa, will represent a lower bound.

Table 5 shows a comparison of the rock mass moduli for each test site based on:

- (i) UCS tests on the drill core in a direction parallel to the axis of the hole  $E_{int}$ ;
- (ii) a  $Q'$  estimated from the drill core and substituted into eqn (4); and
- (iii) tests using the high-pressure dilatometer.

For anisotropic rocks—both hemlo sites and the shale—significant inconsistencies are suspected between (i) and (iii) because the moduli were determined in directions perpendicular to each other. Figure 19 shows a compilation of data based on surface tests [20], to which the current results have been added. For the surface locations the  $E_{dilatometer}$  can be well estimated from  $E_m$ , whereas for the underground tests the  $E_m$  estimate is too low, and  $E_{int}$  provides the better estimate. Obviously considerable care must be taken in selecting an  $E'$  from which  $K_r$  can be calculated. It will depend on such factors as the intact rock modulus, the degree of natural fracturing, stress-induced fracturing, the *in situ* stress and mining-induced stress changes, which themselves are difficult to approximate.

Equation (3) is less sensitive to changes in  $\nu'$ . A value obtained from UCS tests will provide a good first approximation in most cases.

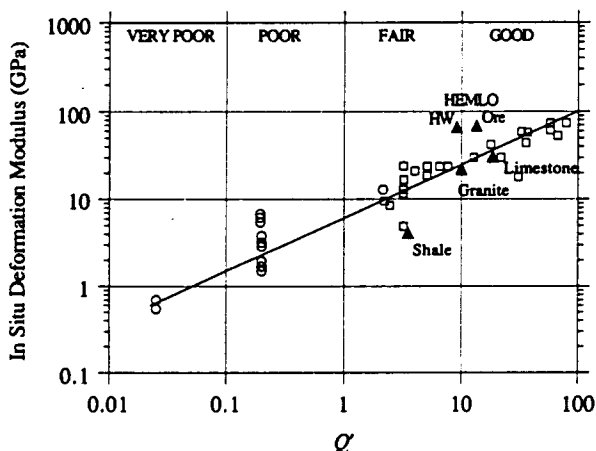


Fig. 19. *In situ* deformation modulus vs  $Q'$  for tests close to the surface [20]. Solid symbols indicate data from this paper.

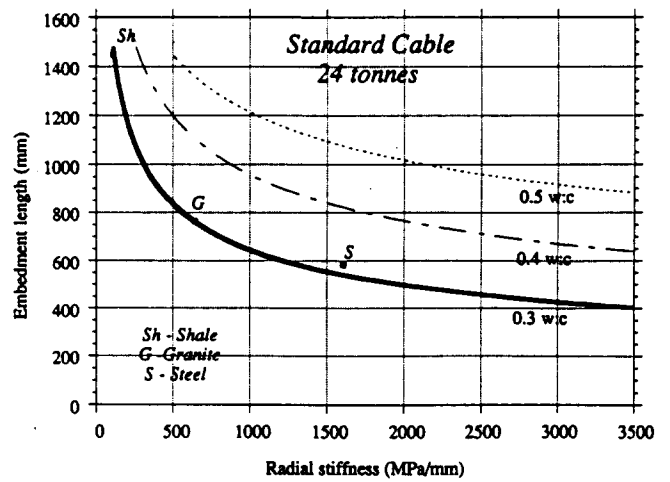


Fig. 20. Projected combinations of radial stiffness and embedment length required to attain a cable capacity of 24 tonnes for a 0.3, 0.4 and 0.5 water:cement ratio grout.

*Guidelines for the improvement of cable bolt systems*

Figure 20 indicates combinations of embedment length and radial stiffness for which the yield of the cable (24 tonnes) will be attained. It is based on the data presented in Fig. 18 and the limited data set existing for a 0.4 water:cement ratio grout. For rock masses that plot above that line corresponding to the water:cement ratio of the grout specified for installation, and remaining above it during mining (see below), optimum cable bolt design is possible using a standard 7-strand cable; so, if low cable bolt capacities are suspected, the explanation must be related to a quality control issue: perhaps dirty cables or a high water:cement ratio grout (i.e. the cable bolt crews adding excess water to the mix). Alternatively, if ground conditions are such that they plot below the appropriate line, then optimum design cannot be achieved using a standard 7-strand cable. In this case two options exist for the operator: either, accept reduced capacities, the degree of which can be estimated from Fig. 18 (see also Ref. [21], Fig. 13); or, adjust the cable bolt system to force higher capacities by using a modified cable geometry (e.g. birdcage cables [22], nutcase cables, cable buttons etc.), adding plates or by using a sanded grout.

*Mining-induced effects*

As indicated in Fig. 21 mining-induced stress changes and associated stress-induced fracturing and spalling can shift the position of a particular rock mass within Fig. 20. Stress-induced fracturing around an excavation can result in very short embedment lengths, so that cable bolts are unable to prevent spalling. In such circumstances plating of the cable bolt at the collar of the hole may be effective.

In the case of mine-induced stress changes, two effects can occur: first, destressing of the ground can cause a decrease in the stiffness of the confining rock mass as it relaxes; second, mining-induced stress changes within the rock mass can cause a change in the radial stress acting across the cable-grout interface, and hence change the frictional resistance which controls the cable

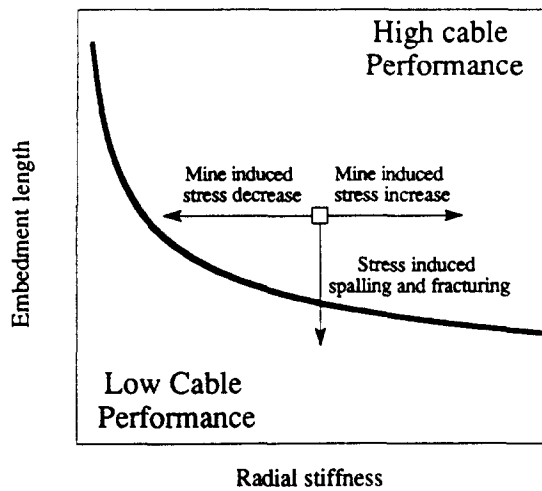


Fig. 21. The effect of mining on the position of a rock mass within Fig. 20.

capacity [23]. Both stress-induced fracturing and mining-induced destressing will reduce expected cable capacities, while a stress increase will maintain or increase them. Using the approach discussed above, it is possible to assess whether field cable bolt failures, especially those where the cables do not appear to have taken much load, are the result of poor ground conditions, or poor quality control during installation. In the case where both are suspected to some degree, it will almost always be cost effective to address the quality control issues first, and then to consider whether it is necessary to alter the cable system to account for poor ground conditions.

**Acknowledgements**—Research funding was provided by the Mining Research Directorate (M.R.D.) under the research contract "Support of Underground Excavations in Hard Rock". Dywidag Inc. provided bars, nuts and couplers. Adam Coulson, Doug Milne, Alain Gendron, Peter Lausch and Delbert Adams provided helpful ideas on aspects of field testing. Jim Paynter supported the test programme at the Golden giant mine, and Donna Cortolezzis organised much of the underground work. Alistair Mathias helped install the specimens.

Accepted for publication 8 January 1992.

## REFERENCES

1. Fuller P. G. and Cox R. H. T. Mechanics of load transfer from steel tendons to cement based grout. *Proc. 5th Aust. Conf. on the Mechanics of Structures and Materials*, Melbourne, pp. 189–203 (1975).

2. Goris J. M. Laboratory evaluation of cable bolt supports. *92nd Annual General Meeting of the CIM*, Ottawa (1990).
3. Bawden W. F., Hyett A. J. and Lausch P. An experimental procedure for *in situ* testing of cable bolts. *Int. J. Rock Mech. Min. Sci. & Geomech. Abstr.* **29**, 525–533 (1992).
4. Potvin Y., Milne D. and Gendron A. Cable Bolt Research Project—Status Report. NTC Internal Report (1989).
5. Hyett A. J., Bawden W. F. and Reichert R. D. The mechanics of cable bolt failure: a laboratory investigation. In preparation.
6. Mehta P. K. *Concrete. Structure, Properties and Materials*. Prentice-Hall, Englewood Cliffs, NJ (1986).
7. Hyett A. J., Bawden W. F. and Coulson A. L. Physical and mechanical properties of normal Portland cement pertaining to fully grouted cable bolts. In *Rock Support and Underground Construction* (Kaiser P. K. and McCreath, Eds), pp. 341–348. Balkema, Rotterdam (1992).
8. Reichert R. D. A laboratory and field investigation of the major factors influencing bond capacity of grouted cable bolts. M.Sc. Thesis, Queen's University, Kingston (1990).
9. Richart F. E. and Bauer E. E. Relations between voids and plasticity of cement mortars at different water contents. *Proc. ACI* **22**, 385–403 (1922).
10. Bazant Z. P. and Sener S. Size effects in pullout tests. *ACI Mater. J.* **8**, 347–351 (1988).
11. Tepfers R. Cracking of concrete cover along anchored deformed reinforcing bars. *Mag. Concr. Res.* **31**, 3–12 (1976).
12. Bentur A. and Mindess S. *Fibre Reinforced Cementitious Composites*. Elsevier Applied Science, London (1990).
13. Bartos P. Review paper: bond in fibre reinforced cements and concretes. *Int. J. Cem. Comput. Ltwt. Concr.* **3**, 159–177 (1981).
14. Bawden W. F., Reichert R. D. and Hyett A. J. Research into the ultimate bond capacity of fully grouted cable support. Interim Report to the Mining Research Directorate (MRD) (1990).
15. Farmer I. W. Stress distribution along a resin grouted rock anchor. *Int. J. Rock. Mech. Min. Sci. & Geomech. Abstr.* **12**, 347–351 (1975).
16. Lutz L. and Gergely P. Mechanics of bond and slip of deformed bars in concrete. *ACI J.* **64**, (1967).
17. Aydan O., Ichikawa Y., Ebisu S., Komura S. and Watanabe A. Studies on interfaces and discontinuities and an incremental elasto-plastic constitutive law. *Rock Joints* (Barton and Stephansson, Eds). Balkema, Rotterdam (1990).
18. ISRM suggested methods for deformability determination using a flexible dilatometer (1985).
19. Franklin J. A. *et al.*, ISRM suggested methods for rockbolt testing. In *Rock Characterisation Testing and Monitoring* (Brown E. T., Ed.). Pergamon Press, Oxford (1981).
20. Fuller P. Cable support of underground openings. Unpublished AMIRA Report (1987).
21. Reichert R. D., Bawden W. F. and Hyett A. J. Evaluation of design bond strength for fully grouted cable bolts. *CIM Bull.* (accepted for publ.).
22. Hutchins W. R., Bywater S., Thompson A. and Windsor C. R. A. A versatile grouted dowel reinforcing system for rock. *Proc. Aust. IMM* **1**, 25–29 (1991).
23. Kaiser P. K., Maloney S. and Yazici S. A new perspective on cable bolt design. Paper presented at the *93rd AGM of the CIM*, Vancouver (1991).